A Design Methodology for Porous Stents to Control Hemodynamics Inside Abdominal Aortic Aneurysms

by

Juan Stockle

A thesis submitted in conformity with the requirements
for the degree of Doctor of Philosophy
Graduate Department of Mechanical and Industrial Engineering
University of Toronto

© Copyright 2018 by Juan Stockle

Abstract

A Design Methodology for Porous Stents to Control Hemodynamics Inside Abdominal Aortic Aneurysms

Juan Stockle

Doctor of Philosophy

Graduate Department of Mechanical and Industrial Engineering

University of Toronto

2018

This thesis presents a methodology to control blood flow conditions inside aneurysm sacs by means of multilayer porous stents. These devices are an alternative for patients with complex endovascular morphologies, specifically, in Abdominal Aortic Aneurysms (AAAs) with short infrarenal necks that are not eligible for Endovascular Aneurysm Repair (EVAR) with traditional devices. Whereas traditional stents isolate the blood flow from the wall, porous stents aim to regulate the flow conditions inside the aneurysm to reduce the risk of rupture, promoting the formation of an Intraluminal Thrombus (ILT) to mechanically protect the wall from flow-induced forces. However, a clear definition of the optimal ILT size, location, attachment type and thickness that lead to the reduction of AAA wall rupture risk is still not well understood. In the event that one of these factors contribute to the increase of AAA rupture risk, porous devices should be designed or customized according to a patient's geometry to prevent undesirable configurations by controlling the hemodynamics inside the AAA sac. Based on this, we conducted our research with the aim of developing a methodology to design porous stents that can induce appropriate blood flow conditions within AAAs. Before developing this methodology, a study focused on the mechanical behavior of the aneurysm wall under different AAA-ILT configurations is performed. This is done to confirm that the presence of the thrombus could lower the forces on the aneurysm wall, and to characterize the effect of partial ILT attachment on these forces. After performing the AAA-ILT mechanical behavior study, we develop a relatively accurate and computationally inexpensive method to model the flow behavior in the AAA when porous stents are used. Given that there are multiple length scales involved (micrometer size pores in a centimeter size artery), a multi-level approach is proposed as a modelling methodology for capturing the hydrodynamic changes across the stent pores without requiring a large number of mesh cells. The detailed simulations through stent pores are carried out to capture the hydrodynamic effects, specifically to study the pressure drop across the stent under different angles of incidence and stent porosity values for a range of physiological velocities typically found in AAAs. Once the flow behavior across the stent is characterized with detailed pore-level simulations, its effect on the flow is modelled as a porous region with known porosity and pressure-velocity curves. This allows us to reduce the computational cost of the simulation by bridging information across multiple length scales. Then, a methodology is proposed to effectively design porous stents that control the blood flow inside the sac within a suitable hemodynamic range defined *a priori*. The method proposed could improve the current decision-making, planning, and outcomes of interventions for any AAA geometry.

Acknowledgements

There so many people to thank for all the support, loving kindness, and enthusiasm they have shown me over the past few years as this thesis has come together; please forgive any oversights or omissions. A few people, in particular, deserve special note.

I am thankful of had the opportunity of working under the supervision of Professor Cristina Amon and her extraordinary group at the ATOMS Lab. She was always very attentive to all my needs, supporting and giving wise advice in challenging moments. My sincere thanks to all the members of my committee meeting for participating and assessing my research project. Their support and questions were crucial for guiding the direction of the thesis. I also would like to extend my gratitude to David Romero who assisted me in many phases of the project, always available and helpful in adverse situations. I want to acknowledge to David James and Iain Currie for welcoming and inspiring at the beginning of this study.

I thank Mario Letelier who always believed in my academic capacities, encouraging me to continue studying and exploring other branches out of fluid mechanics. He has been an influential person in my career and I am happy we crossed paths.

Special thanks to Carla and Laura for their unconditional love and support during this journey. They were always accompanying me in the whole process. Words cannot express my gratitude to them for believing in me and my vision.

Final thanks to CONICYT for the scholarship to pursue my studies at the University of Toronto.

Contents

List of Tables

List of Figures

Chapter 1

Introduction

Aneurysms are an atypical enlargement in the wall of a blood vessel. The development of these enlargements can occur on different sites of the endovascular system, mostly in the brain, thorax, abdomen, and heart. When the dilation is located in the infrarenal zone of the aortic vessel, between the renal and iliac arteries, as schematically indicated in Fig. 1.1, it is called an Abdominal Aortic Aneurysm (AAA). AAAs are classified according to the shape: fusiform when the bulge is symmetrical around the circumference of the aorta, and saccular when the dilation appears preferentially on one side of the aorta.

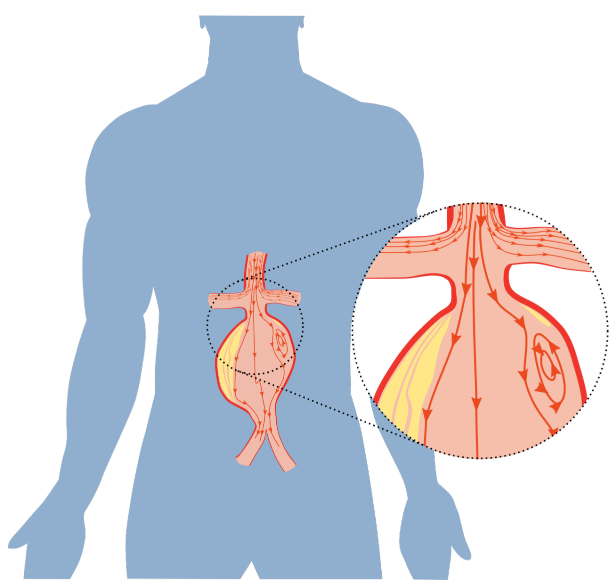

Figure 1.1: Location of the abdominal aortic aneurysm

1.1 Problem Statement

1.1.1 Clinical Situation

Abdominal aortic aneurysm (AAA) affects a significant amount of the population in developing countries. According to data, it takes the life of $4,500$ people annually and has been ranked the 13th major cause of death in the USA [44]. If rupture occurs without the supervision of a specialist, there is about a 10% chance of survival. From the $45,000$ repair procedures performed annually to prevent its progression, approximately 95% of patients survived [39]. The most frequent symptom is abdominal pain, sometimes with the sensation of a throbbing mass but most of the time its presence is asymptomatic. Indeed, people have been diagnosed with this pathology just after a medical examination for other health issues. Unfortunately, its asymptomatic presence delays early detection, making it difficult to treat by means of medical management.

Specialists evaluate preoperative patient characteristics such as age, gender, health, AAA geometry, size, and surgical history to decide an appropriate treatment for reducing rupture risks, and increasing life expectancy. To prevent rupture, a diagnosed AAA is differentiated by its suitability for surgical or endovascular repair based on its maximum diameter or expansion rate measured over time during patient follow-up. However, the use of this diameter as a evaluation parameter for deciding between clinical surveillance or elective repair is controversial due to AAA ruptures reported with diameters below this criterion ($d < 5.5$ cm) [10, 42] and cases with larger diameter expansions without sign of rupture even when the threshold for elective repair has been exceeded. From another side, there are investigations that have pointed out that peak wall stress is a better predictor regardless of the diameter [19, 20, 75]. Since the evaluation of the peak wall stress alone is not enough for accurate prediction, other parameters such as the wall strength, the wall thickness, and presence of ILT structures among others have been added to improve the evaluation of rupture susceptibility [49, 71, 79].

Endovascular Aneurysm Repair (EVAR) with stent-grafts dates back to 1990's, with seminal work performed by Parodi and Palmaz [43], Volodos [77] and Lazarus [31], among others. Following this development stage, the first stent device for endovascular repair was approved by the FDA in 1999. Since then, multidisciplinary groups have been focusing on enhancing the technology by developing tools and accessories that reduce problems peri- and post-operatively. Nowadays, there is a host of FDA-approved devices available, such as the Aptus, Cook, Gore, Medtronic, and Trivascular, among others. Specialists choose a device depending on patient-specific geometrical features, history of surgical procedures, and other factors that contribute to the risk of failure. For instance, the Zenith flex stent-graft shown in Fig.1.2, with three standard versions on the market, is a flexible device restricted to patients having no morphological issues. It includes a trigger-wire used to improve sealing on the infrarenal neck and reduce migration risks. In cases where the patient does not match a standard size, the stent-graft can be customized by changing the dimensional parameters x_1, x_2, x_3, y_1, and y_2, specified in Fig. 1.2.

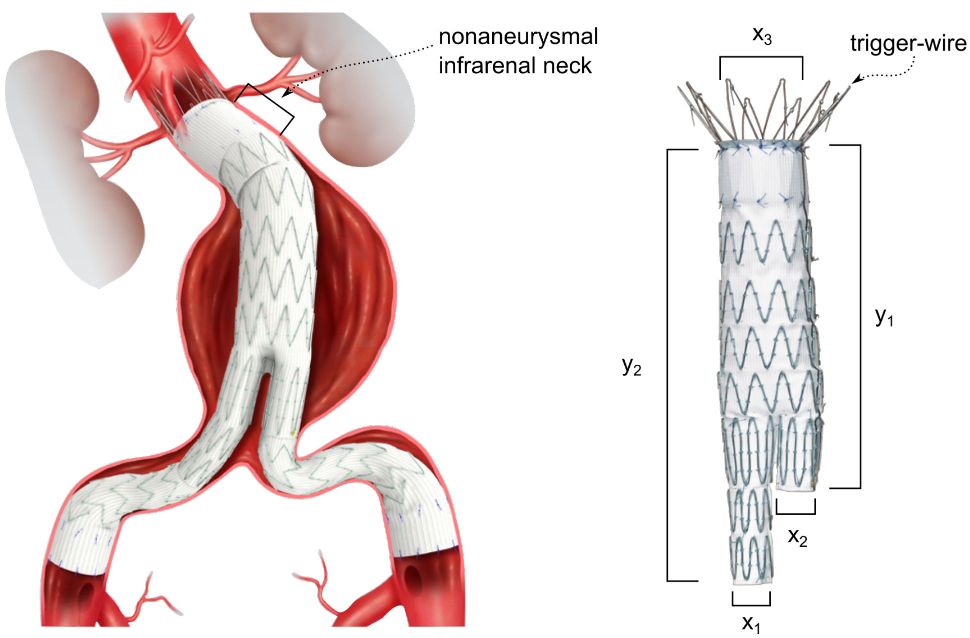

Figure 1.2: Stent-graft by cook, ZenithFlex, picture taken from the Zenith abdominal portafolio

There are patients who do not qualify for EVAR with traditional stent grafts due to morphological characteristics that decrease the rate of success. In particular, patients with a short infrarenal neck are not suitable for treatment with stent-grafts currently approved by the FDA because of insufficient room for adequate sealing. Fenestrated endografts are devices designed to overcome these limitations by extending the landing zones and the insertion of collateral stents that maintain the patency of blood to renal arteries and other side branches. Although these devices were shown to be successful, there are limits to their use, particularly because of the need to customize them to patient-specific anatomies, and also because of device rotations upon deployment that may occlude the renal artery and lead to kidney failure, if not corrected in a timely fashion [58]. According to medical reports, some renal arteries have ruptured after device deployment [76].

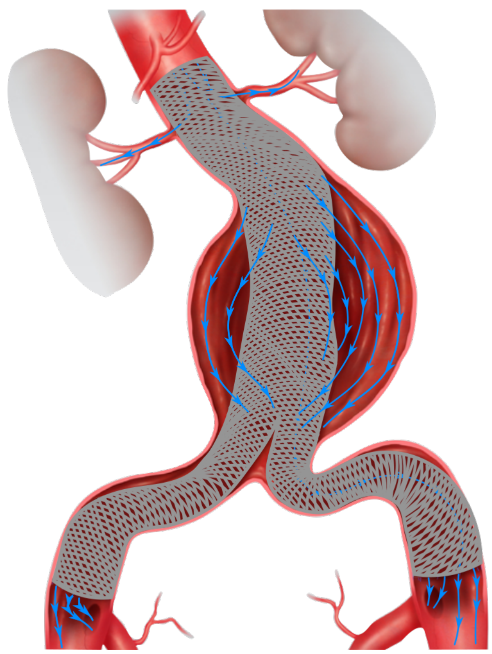

Figure 1.3: Schematic representation of multilayer stent deployed in an AAA.

Nowadays, an alternative device, the multilayer stent, is being used in some jurisdictions of Europe for complex EVAR procedures [26, 46]. Multilayer stents consist of a three-dimensional braided-wire tube composed of several interlocked layers as shown in Fig. 1.3. The main feature of such stents is their permeable walls, which modulate

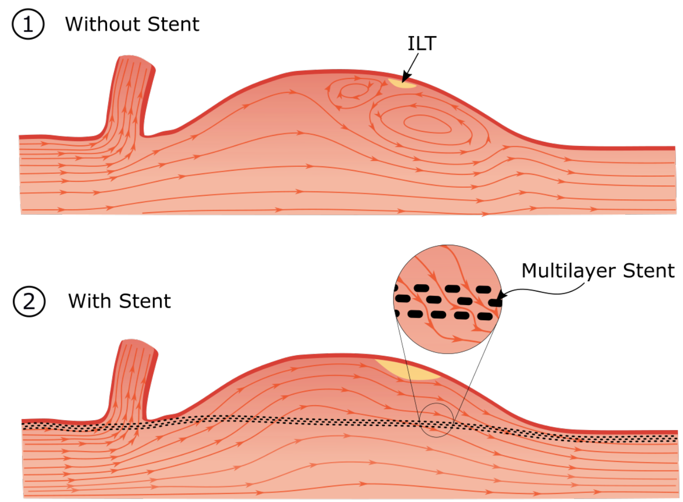

Figure 1.4: Flow changes caused by multilayer stents on AAAs. The figure presents two cases: 1) without stent, and 2) with stent.

blood flow inside the aneurysm sac enabling the formation of ILT, while also maintaining patency to the side arterial branches. Figure 1.4 shows a schematic representation of an AAA with and without stent to observe the changes of blood flow caused by the presence of the multilayer stent. Because of this feature, these devices do not need to be customized to the patient's anatomy and are not affected by deployment rotation issues, potentially providing an off-the-shelf, safe alternative to traditional EVAR devices. Although favorable results about the use of this device in peripheral and visceral aneurysms have been reported [18, 56], there are cases showing the contrary in AAAs [25, 30, 65]. This has motivated us to perform a research project focused on the understanding and impact of multilayer stents on the blood flow behavior inside the AAA sac for improving future designs.

1.1.2 Porous Stents

Interventions with porous stents have been a trend to treat cerebral aneurysms, specially on large or wide neck lesions and fusiform aneurysms. The main purpose of these porous devices, known also as Flow Diverters (FDs) in this context, is to redirect the flow away from the aneurysm wall, reducing rupture risks while still allowing a minimum flow rate inside the aneurysm. As a consequence of the reduced flow rate, the development of a thrombus is likely to occur inside the aneurysm sac where velocities are less intense compared to bulk zones in healthy vessels. Although the aim of porous devices is similar regardless the zone where an aneurysm appears in the endovascular system, the configuration and size of devices change depending on aneurysm type.

Different experiments and computational studies have been carried out to understand the influence of FDs on the blood flow. Peach *et al.* [45] conducted a computational simulation using 6 patient-specific bifurcation aneurysm geometries, reporting a substantial inflow reduction into the aneurysm sac to the order of 50% in all stented cases, leading to reductions of peak and average wall shear stress to values considered normal. In vivo tests on animals were also carried out to evaluate the efficacy of the device in occluding the aneurysm sac. A canine experiment conducted by Darsaut *et al.* [11] reported aneurysm occlusion in 14% of cases after 3 months of follow-up. Another canine study in 21 animals reported incomplete aneurysm occlusion after 3 months of follow-up, achieving shrinkage in all bifurcation aneurysms and sac shrinkage in half of the samples [52].

Computational and experimental research to study the impact of stent porosity on the hemodynamic alterations inside aneurysms has also been performed. Liou *et al.* [34] investigated, numerically and experimentally, the blood flow behavior inside a stented lateral aneurysm anchored on a straight parent vessel. The principal objective was to understand the influence of stent porosity on important hemodynamic variables, notably wall shear stress, pressure, streamlines, vortex, and secondary flow. The hemodynamic variables were compared at different times during a single cardiac cycle for four distinct stent porosities (100%, 70%, 50%, and 25%). The experimental results were in agreement with those from computational simulations in terms of the hemodynamic variables of interest. Surprisingly, the stent porosity did not seem to have an impact on the mean wall pressure, only a 3% difference in the cycle-averaged wall pressure was observed with respect to the unstented case [34]. However, lower flow velocities were found when the stent porosity was decreased, as expected. Thrombosis is likely to occur due to the reduction of flow velocities inside the aneurysm sacs. Therefore, the porosity distribution of the stent should be further studied to promote the growth of ILT structures under controlled environments. Although there are investigations showing either experimental or clinical success after FD installation in cerebral aneurysms, stenosis or occlusion on side branches are complications that need to be addressed for improving post operative results.

Porous stents are not only limited to treat cerebral aneurysms. This approach has also been used in other regions of the endovascular system like in the thorax and perirenal zones [36, 83, 92]. For instance, Zhang *et al.* [92] investigated the performance of bare-metal stents thoracic aortic aneurysms, under single-stent and overlapping-double-stent configurations. The flow conditions were assumed steady-state, laminar and incompressible, and the fluid was modelled as Newtonian. The computational results showed a higher reduction of the WSS on the aneurysm wall with the overlapping configuration compared with the single-layer configuration and the control baseline case (unstented). The peak pressure inside the sac decreased with the presence of the stent, as other researchers have pointed out in similar studies, leading to more uniform pressure distributions than cases without stents. An organized laminar flow with lower recirculation and stagnation zones was observed in the stented case. The authors concluded that the overlapping stent configuration is an effective method to isolate the aneurysm, promoting thrombus formation and reducing the risk of rupture as multilayer stents do. In a similar study conducted by Wang *et al.* [83], under pulsatile flow conditions, the authors performed a Fluid-Structure Interaction (FSI) and CFD simulations to understand the impact of stent deployment and stent porosity on the wall stress and the hemodynamic parameters inside the aneurysm sac respectively. Results showed that the mean time-averaged WSS decreased approx 21% with the single stent and 26% with two overlapped stents, the time-averaged pressure in the sac decreased by 2.4% after the installation of the first stent and $5.1 \pm 0.9\%$ with the second stent in place. Notably, the authors observed that changes in the hemodynamic parameters were insensitive to different overlapping patterns with the exception of the overlapping cases with complete strut alignment. Following up on these findings, multilayer porous stents have been developed to treat aneurysms in different areas of the vascular system with relative success [2, 3, 27, 36, 72]. It is an approach that has not been approved yet due to the lack of thorough data supporting its effectiveness on aneurysm progression. Hence, most publications in the literature point to the need for further investigations into the impact of this device on the hemodynamic environment inside the AAA. Therefore, in order to enhance the understanding of the effect of porous stents on the hemodynamic factors inside the sac, we performed CFD simulations varying the stent porosity distribution to calculate the impact on the blood flow inside the AAA sac.

1.1.3 Simulation Methods

Researches on AAA have been carried out using either analytical, experimental and numerical methods or a combination of them. Analytical studies are scarce due to the geometrical complexity of the system, the non-linearity of the governing equations, and the strong dependence on boundary conditions that increase the difficulty of solving the equations of motion. As an alternative, experimental setups mimicking patient endovascular geometries and flow conditions have been useful to study problems quite difficult to solve with the mathematical tools available nowadays. However, experiments cannot be easily implemented for pre-surgical planning, making them impractical from a clinical perspective. Fortunately, with the availability of high-performance computing resources and software applications, computer simulations with complex geometries and non-linear behavior are attainable in a reasonable time. These methods are suitable for the study on patient-specific cases with geometries obtained from computed tomography angiography images.

To understand the impact of boundary conditions and modelling assumptions on study results, sensitivity or parametric studies have been performed on aneurysm models while monitoring changes in the parameters of interest. For instance, Chandra *et al.* [9], monitored the changes on the maximum principal stress, maximum principal strain, pressure and wall shear stress distributions under different flow boundary conditions. The same authors also investigated the effect of including the compliance of AAA walls by running FSI simulations to observe changes in the same parameters compared to cases that assumed rigid walls. Results showed that a so-called one-way (decoupled) FSI approach provides reasonable accurate biomechanical assessment employing less computational effort, leading to differences in peak principal stress, principal strain, and WSS of 14%, 4%, and 18%, respectively, compared to the fully coupled FSI analysis. To obtain reliable solutions saving computational time, different aspects of the computational modelling have to be analysed before making the physical assumptions. In our study focused on the mechanical behavior of the AAA with and without ILT structures, explained in more detail in next chapter, we used the argument explained above to perform the simulations using static and one-way FSI approach assumptions to evaluate the susceptibility of AAA wall rupture.

Flow regime is another condition that is taken into consideration when simulating blood flow through AAAs. Given that the blood flow is pulsatile with peak Reynolds numbers in the range from laminar, transitional and turbulent regimes, ($262.5 \leq Re_{peak} \leq 1575$), an analysis of the impact of the regime assumption is important for ensuring accuracy. In the literature there are works that have assumed laminar regime for the entire pulsatile cycle arguing that the laminar regime dominates over the pulsatile cycle [60, 83]. For instance, Shek *et al.* [60], assumed laminar regime through stented AAA with different limb configurations to study their effect on flow-induced forces acting on the stents (coronal, sagittal and axial force directions). In this thesis, we follow previous work in assuming rigid AAA walls and laminar flow throughout the cardiac cycle [64].

In particular, the laminar flow assumption closely mimics real conditions in blood vessels with porous stents [2, 27, 81].

Regarding the AAA geometry, there are studies using either 3D patient-specific, or hypothetical 2D/3D geometrical models. Patient-specific geometry models have been used for different study purposes. There are groups of researchers more focused on simulating aneurysm deformation under the action of fluid forces to evaluate rupture susceptibility from the mechanical point of view [78]. Others have focused on the risks and performance of device implantation pre-, intra-, and post-operative [58, 60, 83]. For instance, Sanford *et al.* [58] simulated the mechanical behavior of fenestrated stent-grafts used for endovascular repair on patients with short infrarrenal necks using four AAA patient-specific geometries to predict rotation of grafts during implantation. On the other hand, studies using hypothetical 2D and 3D geometries have been performed to better understand the impact of geometrical factors on the flow and the mechanical behavior of the wall [17, 21]. For instance, Elger *et al.* [17], from a mechanical point of view, studied the impact on the AAA wall stress in hypothetical axisymmetric AAAs of curved shapes showing that the larger stresses occurred in cases of small AAA curvature while Finol *et al.* [21] investigated the effect of aneurysm asymmetry on wall shear stress, from a fluid point of view. The results from Finol *et al.* [21] showed that increasing the asymmetry of the AAA geometry increased the WSS caused by the predominant effect of the inertial over the viscous forces that lead to the formation of secondary flows. Other examples are investigations aimed to characterize the dynamic changes of important parameters of the flow as the AAA progresses. For instance, the work conducted by Salsac *et al.* [57], investigated the changes on the WSS, the WSS gradient and the vortex for different AAA shapes varying systematically the aspect ratio L/d and the dilation ratio D/d where D and L are the maximum inner diameter and length of the AAA bulge and d is the inner radio in the parent vessel. The computational results showed good agreement with the experiments performed in symmetric AAA models on an oscillatory flow loop. The investigations discussed above were used to understand the impact of the geometric parameters on the hemodynamic changes inside the AAA sac without stent, especially on the hemodynamic parameters of the wall (WSS and pressure distribution). Thus, this information was used to understand the hemodynamic fluctuations to be controlled by a porous stent.

Another important consideration for computational simulation studies of AAAs is the rheological model for the blood. Blood is a fluid composed by platelets, red and white blood cells, and plasma that carries a mixture of proteins, enzymes, nutrients, waste, hormones, and dissolved gases. Platelets, also known as thrombocytes, play a vital role in the coagulation cascade, which is affected by local shear rates. As a result, blood has a non-linear rheological behavior. For shear rates above 100 s^{-1}, the blood viscosity is considered to be constant, whereas for values below this threshold, the viscosity experiences an exponential increase related to the concentration of red blood cells. However, below 100 $s^{-}1$ experiments to characterize the viscous behavior as function of the red blood cells concentration have not been definitive, leading to a wide variety of rheological models for blood with no consensus [90]. In large arteries, blood experiences shear rates above and below of 100 $s^{-}1$ depending on the size and shape of arteries, and the frequency of the pulsatile wave. For instance, in healthy aorta, the shear rate is above this threshold thus the blood can be modelled accurately with constant viscosity. However, in the presence of an aneurysm, the fluid flow experiences deceleration when entering the sac leading to non-Newtonian behavior in places where the viscosity decreases as consequence of reduction on the shear rate. But, as the nature of blood flow is pulsatile, the short time experience of low shear rate could justify the assumption of considering blood as Newtonian fluid.

Different studies have tried to clarify the importance of the shear-thinning behavior of blood on parameters of interests. For instance, by varying constitutive blood models, Lee and Steinman [32] were able to understand the effect blood rheology on flow parameters such as the time-averaged WSS or oscillatory shear index (OSI) on a carotid bifurcation. The results showed that the election of the fluid model is not crucial because important flow parameters are not vastly affected by the choice of blood rheology models, however this depends on the particular goals of the study. Among other numerical simulation studies, the selection of constitutive models and the effect of mesh resolution have been of particular interest. For instance, Cavazzuti *et al.* [8] showed the importance of employing non-Newtonian models to avoid under or overestimation of hemodynamic parameters, as compared with results obtained assuming Newtonian flow. In their investigation, the authors concluded that the non-Newtonian approach makes it possible to obtain a better understanding of the flow dynamics and evaluate the stent performance accurately. However, from the perspective of the aim of our study, there is no need to use non-Newtonian flow behavior to model the blood flow because we are not interested in the impact of the shape of the stent struts on the shear stress behavior of the fluid flowing though the stent. Besides, according to a results presented in Chapter 3, the pressure drop trough the porous media, an effect we want to model, is not significantly changed by the fluid model. Moreover, the frequency of the pulsatile cycle used in our simulations is considerably short, approx 1.2 second, therefore, a Newtonian model for the blood flow is an acceptable assumption for the purposes of our study.

Simulation methods are used depending on resources, expertise of users, and objectives to reach. For the research presented in this thesis, we utilize a numerical approach using an element-based finite volume method to solve the momentum equations. Since the main goal of the thesis is to develop a methodology for finding suitable stent designs for the improvement of EVAR on complex AAAs, we do not need to use patient-specific AAA geometries for performing proof of concept studies. Instead, we employ an hypothetical 2D AAA model for running simulations and result analysis. We employ steady-state and pulsatile flow conditions for simulating the blood flow, assuming laminar conditions for the blood as other researchers have employed in their works [60, 83] and due to the fact that the stent laminarizes the fluid inside the AAA sac [64]. The fluid is considered Newtonian due to the short frequency of the pulsatile cycle even though there are instances in which the shear rate inside the sac is below the threshold values for the assumption of Newtonian fluid behavior. In addition, the shear-thinning models for the blood have shown discrepancies between them with no consensus[90], leading to over or underestimation of some hemodynamic parameters and increasing the complexity of the problem by setting these model for the fluid. The assumptions of the problem study on this thesis do not affect in any way the intelligent methodology approach developed for finding suitable stent configurations. Before carrying out the development of an intelligent approach methodology, we perform a simulation focused on the impact of different ILT attachment configurations on the wall stress of the AAA. This prior study is intended to find ILT formations that could be detrimental to the AAA against the fluid forces. In case of finding innappropriate ILT configurations, the intelligent approach methodology should consider a flow restriction for avoiding them.

Computational Considerations

Modelling fluid flow through porous media is computationally expensive and complex from a mesh generation perspective. Dense meshes are needed in these domains since the scale of the pores in stents are order-of-magnitude smaller than the size of aneurysms. In fact, the wide range length scales between the stent pore and the AAA diameter, around 10^{-5} m and 10^{-2} m respectively, requires an experienced specialist to create an adequate mesh with smooth transitions for obtaining convergence and stability in the simulations. For example, a minimum cell density of approx. $10,000$ cells/mm^3 was needed for obtaining mesh independence of aneurysm inflow of a stented carotid artery [45]. Consequently, pre-operative evaluations with these settings would be impractical from the clinical perspective due to the expensive computational cost and the long lead time patients have to wait. To overcome this issue, alternative techniques for meshing these devices have been developed to decrease computational effort for faster calculation with reliable results. For instance, Raschi *et al.* [51] developed a strategy to study flow through Flow Diverters using a Porous Medium Method (PMM). This decreases the computational time compared with the conventional immerse porous method that employs a detailed meshing of the pores of stents. The results showed that PMM provides accurate hemodynamic results when the FD was placed on non curved aneurysms. The disagreement occurred as a consequence of assuming the permeability coefficient constant along the devices which underestimates the pressure drop effect of the flow in the stent. In our research, we use the same approach used by Raschi *et al.* [51] to model the presence of the stent, but notably it incorporates stent porosity changes in concert with model coefficients, thus making it generally applicable and more accurate.

1.1.4 Modeling of Physiological Structures in Abdominal Aortic Aneurysms

Over the past few decades, researchers have developed mathematical models to predict AAA growth to be useful in diagnosis of patient-specific cases. For instance, Watton *et al.* [84] developed a mathematical tool that predicts the evolution of AAAs by adjusting the parameters of a non-linear model. The remodelling was correlated with variations on the biological structures, influenced by the increase of collagen that compensates the loss of elastin on places where AAA enlarges. In a recent work, also conducted by Watton *et al.* [85], results showed agreement with reported enlargements observed on patient-specific AAA cases. Interestingly, they found that the maximum diameter grows exponentially, stiffening the wall of the AAA as the volume increases. Besides the importance of using AAA growth models [84], patient-specific geometries [70], physiological pulsatile velocity/pressure waveforms [29], and the ongoing development of more sophisticated simulation methods for fluid-structure interaction [91], significant interest has been given to more accurate material models for aortic and ILT tissues [50, 73, 74].

In an effort to obtain reliable and accurate constitutive AAA models used to predict deformation, stress distribution, and other parameters using computational software, researchers have performed mechanical tests using excised patient specimens [14, 23, 38, 50, 74, 80]. Recent studies have used hyperelastic material, Mooney-Rivlin, Fung, Ogden, Polinomial and others, to model the non-linear mechanical behavior of AAAs with more accuracy. For instance, Raghavan and Vorp [50] tested 69 freshly excised pieces of AAA using uniaxial tensile probes to obtain the stress-strain relationship, assuming homogeneous, incompressible, and an isotropic pseudostrain energy density function. One of the goals of this study was to calculate the variability of maximum wall stress by changing the model parameters obtained from the excised samples. The results showed negligible differences in terms of the peak stress when the hyperelastic parameters corresponding to each physiological specimen were varied, supporting the extensive use of this model to other patient-specific or hypothetical cases without much concern about the variability of the mechanical properties of specimens. Hence, in our research, we use the model developed by Raghavan and Vorp [50] to study the mechanical behavior on hypothetical AAAs.

In addition to the development of constitutive equations for modelling AAAs, attention to the mechanical behavior of ILTs, structure attached to the aneurysm wall, has been also the focus of researchers. These physiological structures are found in more than 75% of AAA patients [24], need to be considered into mechanical behavior studies to improve predictability of calculations derived from deformation fields. The importance of including the ILT in our study relies on the fact that porous stents allow recirculation of blood inside the AAA sac, reducing blood velocities inside aneurysm sacs thus promoting ILT formation. Therefore, previous works on ILT onset, evolution, and mechanical properties are discussed below.

ILT grows with the enlargement of the AAA sac due to hemodynamic changes that trigger a cascade of bio-chemical processes that involve the plasma, proteins, red blood cells and the endothelial cells lining blood vessels. ILT is formed in the luminal surface of the aneurysm sac preferable on zones where ILT already exists. It is layered in annular shapes categorized depending on the microstructure of each transmural layer. At later stages, three categories can be identified, luminal, medial, and abluminal layer as indicated in Fig. 1.5. ILT mechanical properties have been tested to characterize, model, and understand its behavior under mechanical loads [73, 82]. They depend on the orientation of fibers in the collagen network of the ILT and have been modelled as hyperelastic materials assuming isotropy in most of works [73].

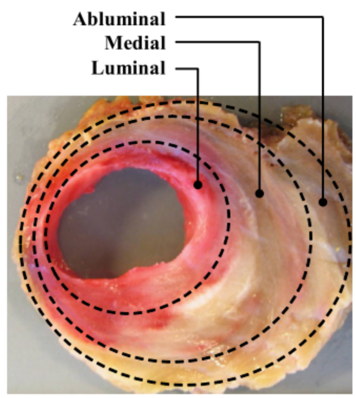

Figure 1.5: Cross section of the bulk ILT tissue harvested from elective AAA repair, where luminal, medial, and abluminallayers are indicated. ILT picture taken from Gasser *et al.* work [23].

The role that ILT plays in the protection of the AAA wall is still unclear and has been focus of debate in the research community [15, 48, 53, 55, 69, 86]. There are researchers who point out that the structure helps to redistribute the stress on the artery wall, protecting the wall from the pressure and shear stress acting on the luminal surface of the aneurysm, [15, 53, 86]. For instance, Di Martino *et al.* [15] studied the effect of ILTs on the artery wall stress distribution by varying their parameters model. Fresh pieces of ILT were taken from seven patients and tested using uniaxial tensile probes. The results were used to build the ILT model, which was then incorporated into computational experiments. At the same time, seven physiological cases were set into a mechanical software in order to contrast them with a base case that does not include the ILT model.

According to the computational results, the ILT protects the artery wall: in the cases that included the ILT, the wall stress distribution decreased. It was also observed that changing the physiological constants obtained from the tensile probes did not lead to wide dispersion in the stress distribution; the maximum variation found for the seven cases was 5 %. In contrast, other researches have showed that departures from the idealized conditions used in previous studies, e.g., the presence of internal cracks on the ILT, specifically the ones reaching the aneurysm walls, could lead to an increase of 30% on the wall stress of the AAA compared to intact ILTs [48, 55]. Also, the presence of liquid-phases at the AAA-ILT interface have been reported, suggesting that ILTs are not always completely attached to the aneurysm wall. This feature, typically found in thick ILTs, could play a critical role in the enlargement and rupture of AAAs [22, 69]. The foregoing discussion suggests that an understanding of ILT formation and attachment process under simulated physiological conditions might be needed to settle the debate about the protective role of ILT. Hence we look at previous investigations focused on formation and growth of ILT structures to understand the processes and the flow dynamics that are involved in this phenomenon.

The formation of ILTs is related to the coagulation cascade process, which is triggered by platelet activation [37]. This first step leads to a tissue primarily composed of a fibrin mesh, including blood cells, aggregated platelets, blood proteins, and cellular debris. In an effort to predict ILT growth on AAAs, Biasetti *et al.* [5] studied the fluid-wall interaction and the effect of vortex structures on the ILT formation by combining biochemical and fluid dynamic models. Two different sites of exposed subendothelium, where platelets adhere to trigger the coagulation cascade process, were analyzed to discard their influence on the ILT growth. The results showed that flow vortex structures play an important role on the spread and deposition of components resulting from biochemical reactions. The combined effect of the subendothelium site and the recirculation zone produced by the vortex structures allows thrombin convection to distal zones of the

AAA, maintaining the transport of biochemical products to the aneurysm sac.

Other researchers have also studied these phenomena [35, 40, 87, 89]. For instance, Xu *et al.* [89] studied the stages of thrombus formation using a multiscale formulation. A cellular Potts model was applied to describe platelet and blood cell aggregation (discrete variables), and partial differential equations were used to describe the blood flow and kinetics of coagulation reactions (continuum variables). For computational simplification purposes of comparison, a parallel plate chamber was created as a model of the vessel wall. The computational results showed good agreement with the experimental findings. The authors concluded that the shape acquired by the thrombus during its formation affects the flow behavior. Another study, conducted by Moiseyev *et al.* [40], investigated thrombus formation but focused principally on the second stage of the coagulation cascade. Based on a mesoscopic model, three parameters (thrombin and plasmin concentration, and local shear rate) were varied to understand their impact on thrombus growth. In contrast to [89], this investigation considered activated platelets and the release of thrombin into the blood plasma. The results showed that the three parameters affect the mechanical properties of the thrombus, and it was possible to determine the ultimate strength of the clot based on the number of cross-links, which in turn depends on the shear rate during deformation.

These works [40, 89] describe the physiological formation of the thrombus as a phenomena characterized by biochemical reactions, biomechanical interactions, biotransport phenomena, residence time of particles (activated platelets), and flow shear rate values, among other factors. A complete understanding of thrombus formation is difficult to achieve because of the multidisciplinary effort involved which is conducted on both the micro and the macro scales, and as such we considered it outside the scope of our work. In connection with our research, this information is relevant to address a potential need for controlling ILT formation; these parameters could be added to the intelligent approach methodology as part of the required hemodynamic targets.

The focus of our investigation is evaluating the performance of multilayer porous stents for promoting suitable hemodynamic conditions inside the AAA sac. From this perspective the above literature review is relevant as it assists in simplifying the present study. We focus on the behavior of flow parameters such as the wall shear stress (WSS) and wall shear stress gradient (WSSG) as these factors have been used to predict ILT formation and risk of AAA wall rupture from a macroscale point of view. However, we will not attempt to model the ILT formation process.

1.2 Research Objectives

The blood flow pattern inside aneurysm sacs with porous stents depends both on the patient's endovascular geometry and on the stent characteristics. However, nowadays there are no guidelines for determining which type of stent design is most efficacious for a given patient-specific geometry. Thus, to improve outcomes of EVAR using porous stents, further research studies that focus on how stent porosity impacts the hemodynamic patterns inside AAA sacs are needed. Furthermore, recent reports have shown significant differences in outcomes when using porous stents for endovascular repair of cerebral aneurysms and abdominal aortic aneurysms, calling into question the hypothesized mode of action of porous stents. To improve our understanding of the mode of action of porous stents, modelling and simulation approaches are needed to conduct computational studies that elucidate the effect of the stent porosity profile on the hemodynamic inside the AAA. To this end, the research plan discussed in this section involves a sequence of independent studies into the mechanics and flow dynamics of AAAs with porous stents, followed by the integration of these findings into a comprehensive methodology for the design of porous stents.

The intraluminal thrombus, commonly encountered inside the AAA sac, is a physiological structure whose formation is altered by the presence of porous stents. In this context, porous stents should be designed to induce appropriate flow field patterns inside the AAA sac to ensure ILT onset and growth without increasing aneurysm wall rupture risks, and that the ILT themselves are considered beneficial with respect to patient outcomes. However, the debate about the role ILT structures play on the prevention of AAA wall rupture is still unclear. From a mechanical point of view, the ILT serves as a shield against the mechanical forces of the blood flow, but their uncontrolled growth could lead to ischemic hypoxia, degrading the mechanical properties of the AAA wall and increasing the risk of wall rupture. Moreover, CT scans have shown that ILTs are not always fully attached to the AAA wall, and in some cases not even partially attached [22, 69]. Since the focus of this investigation is to control the hemodynamic field inside the sac using porous stents, a study to understand the impact of partial or incomplete ILT attachments on the stress of the AAA wall is warranted. In this study, different ILT attachment modes are compared to ascertain the effect of the attachment modes on the stress on the AAA wall. If partially attached ILTs are harmful to the AAA wall, the porous stent configuration should be designed to prevent such ILT scenarios.

Other factors that contribute to a reduction in AAA wall rupture risks can be studied from a fluid perspective. An efficient treatment of AAAs depends in part on the fluid flow conditions inside the sac. These flow conditions could be controlled to remain within target ranges established by medical specialists through the design of patient-specific porosity profiles for the stents. This can be accomplished, as long as the impact of the stent on the flow field can be modelled. However, modelling and simulation of porous stents is challenging, mainly due to the wide range of length-scales involved, from micrometer-sized pores to the centimeter-sized aorta. This range of length scales increases the complexity of domain discretization and mesh generation, a key step for any successful CFD simulation effort. Hence, computationally efficient approaches for simulation of fluid flow in porous stents are needed. Indeed, this problem has been discussed in recent congress organized by the scientific community working on the area [33]. To improve the models of stent devices and their prediction of the hemodynamic parameters inside the sac, we conducted a CFD study to quantify the effect of porous stent configurations on the hydrodynamics across the stent. This research is intended to establish a mathematical relationship between flow velocities seen by the stent with the pressure drop across the stent thickness. The relationship, once known, allows us to model the presence of the stent through its effect on the fluid flow field, reducing the computational cost of the simulations by avoiding the need for meshing a computational domain across multiple length scales. Thus, the simulation setup is less complex and less computationally expensive compared to a comprehensive simulation model that includes both the AAA and the detailed pore structures of the stent. Due to the reduced computational expense and simulation time, this modelling choice will enable pre-operative planning based on patient-specific CFD simulations, in which flow behavior and forces could be compared using different stent configurations. Through this mean, inappropriate hemodynamic scenarios yielded by some stent configurations could be prevented, thus reducing the chance of AAA wall rupture.

The previous works, described in the above paragraphs, are carried out to understand the ILTs protective role under incomplete ILT attachment scenarios and the impact of the stent porosity on the blood flow conditions inside the AAA sac. This information on its own is not useful for assisting clinical decision making during pre-surgery planning, because determining the stent porosity distribution that would result in the best outcome for a given patient-specific geometry is not an intuitive process. Thus, to improve the EVAR practice using porous stents, a methodology is proposed to find suitable stent configurations for improving the hemodynamic conditions inside the AAA sac. This intelligent approach iteratively uses results from CFD simulations to systematically modify the porosity distribution of the stent until hemodynamic targets specified *a priori* are met. This methodology has the potential to improve treatment of AAAs with porous stents, as the proposed methodology provides model-based guidelines to design patient-specific stents that meet the hemodynamic targets defined by physicians and surgeons.

1.2.1 Specific objectives

- Study the impact of varying ILT attachment types on the stress distribution on the AAA wall.
- Develop a computational modelling approach that efficiently considers the multiple length scales that are relevant for fluid flow phenomena in AAAs treated with porous stents.
- Study the influence of the stent porosity on the hemodynamic environment inside aneurysm sacs.
- Formulate a model-based methodology for the design of porous stents for AAA repair.

1.2.2 Expected Impact

While the previous investigations on porous stents have made important contributions toward the characterization of blood flow inside aneurysm sacs, there are very important limitations that leave extensive opportunities for improvement in the field. These are summarized as follows:

- Elucidation of the protective role of ILT that are only partially attached to the AAA wall. Our research contributes both to the understanding of the protective role that ILT has on the AAA wall, and to the improvement of EVAR treatments with porous stents. In particular, our interest is to know if partially attached ILTs lead to increased AAA wall stress. This is particularly important, considering that the hypothesized mode of action of porous stents is to organize the flow patterns and promote the growth of ILTs to protect the AAA wall from flow-induced stresses.

In this context, the present study provides more evidence about the protective role an ILT could have on the AAA wall from a mechanical point of view. In the case of finding that partial ILT attachments do not lead to the increase of stress on the AAA wall, the ILT formation could be an advised characteristic to promote inside AAA sacs by mean of porous stents to prevent AAA wall rupture.

- Development of a methodology for modelling porous stents. A multi-level approach was developed, modelling the pore-level behavior of the stent for different configurations in a range of physiological velocities. These results were employed to represent the effect of the stent on the flow as a porous medium with known model parameters. Therefore detailed flow simulations of the hemodynamics inside the AAAs can be studied with low computational cost and without convergence and stability issues that occur in full multi-level model simulations.

- Development of an intelligent approach methodology for optimization of porous stents. The method allows for the design of porous stents that achieve specific hemodynamic conditions selected by the surgeon. The models can also be used to analyse how sensitive the stent configuration is to changes on the prescribed hemodynamic target, which then allows for an evidence-based prognosis to be given. This has the potential to significantly improve clinical practice and the design of new stent generations for both general use and for specific patients.

1.2.3 Structure of the Thesis

This section describes the document organization and provides a brief description of topics discussed in each chapter.

Chapter 2 focuses on furthering the understanding of the role that intraluminal thrombus plays on the AAA wall, specifically evaluating the impact of ILT attachment types on the peak stress and stress distribution along the AAA wall. Both the ILT and the

AAA geometry are simulated under two boundary conditions for different ILT attachment configurations. Then, a comparison analysis to discuss the susceptibility of AAA wall to rupture under the simulated conditions is carried out taking into account a base case which does not include the presence of ILT structures on the aneurysm.

Chapter 3 presents the modelling of the effect of the stent on the fluid flow field. Sensitivity analyses are carried out to capture the effect of the wide-screen angle of the stent pore and the angle of incidence with which the fluid impact the stent for different flow velocities. Consecutively, a proof-of-concept study using steady-state and pulsatile flow conditions is performed to understand the impact of the stent configuration on hemodynamic factors inside the AAA sac.

Chapter 4 presents the proposed methodology for designing porous stents using the simulation models discussed in Chapter 3. Sensitivity analyses are conducted to describe and verify the methodology, and proof-of-concept studies are conducted to illustrate its capabilities.

Chapter 5 summarizes research contributions, discusses its limitations, and Chapter 6 presents some possible directions for future work.

Chapter 2

Impact of Partial Intraluminal Thrombus Attachment

2.1 Introduction

The formation of ILT could increase the chances of AAA wall rupture if the fluid flow conditions inside the AAA sac are not appropriately controlled. The flow control should be intended to promote hemodynamic environments that efficiently stop the pathology. Thus, porous stents need to be designed not only to reduce blood velocity inside the AAA sac, but also to induce flow behaviours that prevent AAA wall rupture caused by inappropriate ILT formations. If a porous stent is not well designed to control the blood flow behavior, ILTs could be formed inappropriately, increasing the AAA growth rate that lead to unsuccessful treatment of the pathology [67]. Indeed, researchers have pointed out that the unbalanced ILT growth causes hypoxia on the aneurysm wall that deteriorate the mechanical properties of the AAA wall [22, 69], specially observed in thick ILTs. Additionally, other specialists have also reported patient-specific cases with ILT structures that are only partially attached to the AAA walls, e.g., [22, 48, 55, 69], with unknown consequences on AAA wall integrity.

Since the main goal of our investigation is to create a methodology able to find optimal stent configurations for the efficient control of the blood flow environment inside the sac, a study focused on the impact of the ILT on the protection of the AAA wall is performed to determine ILT configurations that might be undesirable from a mechanical point of view. Therefore, this chapter is focused on the study of the mechanical impact that different ILT attachment configurations cause on the stress distribution of the aneurysm wall. To meet this research objective, FEM simulations were carried out using the ANSYS-CFX commercial software to model an hypothetical AAA and ILT structures with full control of the geometrical variables. To evaluate the impact of ILT on AAA wall stress distribution, different ILT attachment modes were tested. In other words, the attachment areas and friction factors (varied from 0.1 to 0.3) between the ILT and the AAA wall were varied to understand their impact on the AAA wall peak stress and stress distribution. The mechanical properties of the AAA and ILT were included in the computational model using hyperelastic constitutive equations derived from patient-specific tensile probes reported in the literature, [50, 73]. To calculate the stress distribution and peak stress, two different force conditions acting along the luminal surface of the system were used. For comparison purposes, an AAA case without ILT was employed as baseline.

2.2 Methodology and Material models

A Computational Solid Stress (CSS) and Fluid-Structure interaction (FSI) were carried out employing hypothetical arterial geometries to calculate the stress distributions on the AAA wall. Since these physiological structures can be assumed isotropic and path-independent, i.e, their mechanical properties are identical in all directions and their deformation depends only on their initial and final states, a second order Moonley-Rivlin material model is employed to model the mechanical behaviour using the strain energy function shown in Eq. 2.1.

$$W_n = a_i \left(I_k - 3\right) + a_j \left(I_k - 3\right)^2 \tag{2.1}$$

where a_i and a_j are the material coefficients obtained from excised tensile probes of patients [50, 73], and the I_k the invariant of stress tensor. Table 2.1 shows the values of the hyperelastic parameters obtained from those mechanical testing that we used to set the numerical software.

Table 2.1: Parameter values set into ANSYS-CFX for modelling the mechanical behavior of the physiological structures

SEF	a_i (N/cm^2)	a_j (N/cm^2)
W_{AAA}	17.4	188.1
W_{ILT}	7.98	8.71

2.3 Hypothetical Geometries

Both CSS and FSI simulations were performed using hypothetical AAA and ILT structures shown in Fig. 2.1. Figures at top and bottom of Fig. 2.1 represent complete and incomplete ILT attachment cases, respectively. The dashed line at the AAA dome, Fig. 2.1 (b), constitutes the detached portion of the ILT upon which a friction coefficient is applied. To test the impact of these attachment types on the protection of AAA wall, a control case without including the ILT was also simulated.

Five different areas of attachment were studied, from fully detached (0%) to fully attached (100%), as illustrated in Fig. 2.2, were studied. Three friction factor coefficients (f = 0.1, f = 0.2, f = 0.3) were varied in every incomplete attachment study case.

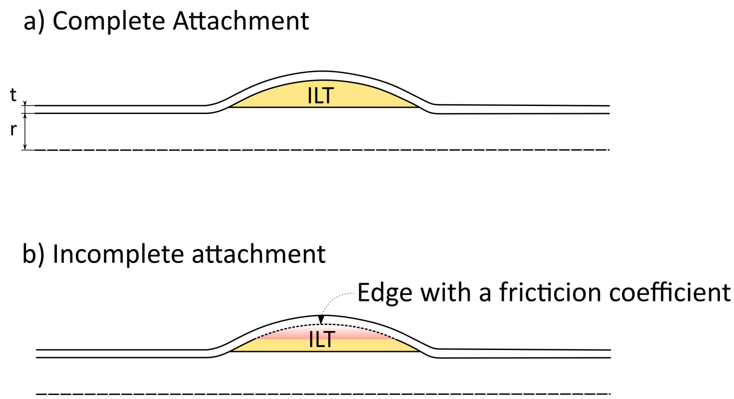

Figure 2.1: Hypothetical AAA and ILT geometries with different attachment types

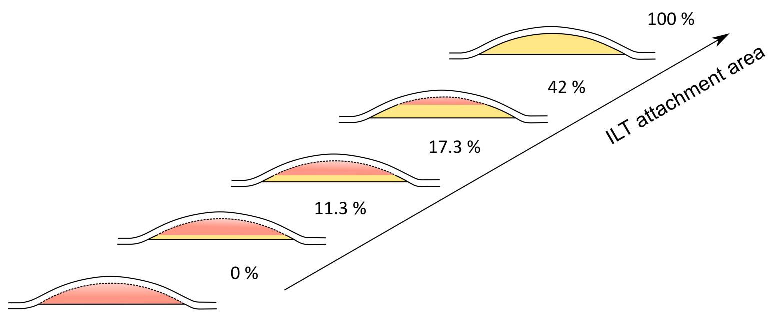

Figure 2.2: Different types of attachment areas: The pink portion represents the ILT portion not attached to the AAA wall, whereas the yellow is the attached portion to the AAA wall.

2.4 Boundary Conditions

A spatially uniform pressure of 120 (mm) of Hg was used as boundary condition for the CSS study and a physiologically peak systolic inflow of 0.5269 (m/s) was defined at the inlet for the FSI study. A same value of density was assumed for both physiological structures, $\rho_s = 2,000$ (kg/m^3) while keeping a constant AAA wall thickness of $t = 1.5mm$ and fixed extremes as constraint. The fluid density and dynamic viscosity of the fluid were set constants, $\rho_f = 1,050$ (Kg m^3) and $\mu = 0.0035$ (Pa s) respectively. A high resolution advection scheme and a residual target of $1.0 \cdot 10^{-4}$ were set for solving the equations of motion. Due to axial symmetry of the fluid and the structures, the problem was calculated using a quarter of the whole 3D domain. Mesh independence analysis was also carried out resulting in a minimum of 68,100 number of elements for the fluid and

59,034 elements for the AAA and ILT domain. Attachment types and friction coefficients are varied to to determine the effect of ILT attachment modes on the AAA wall.

2.5 Results

The results of these computational simulations are plotted in Fig. 2.3. More specifically, the values of the peak wall stress for different types of attachment area (incomplete 0%, 11.3%, 17.3%, 42% and 100%) as illustrated in Fig. 2.2 and for different friction factor values (f = 0.1, f = 0.2, f = 0.3) are presented.

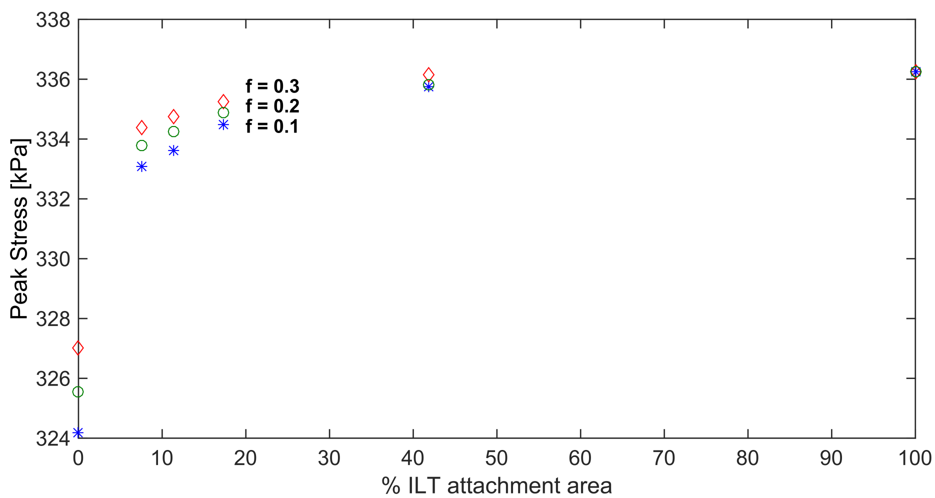

Figure 2.3: Peak stress for different percentages of ILT attachment areas and friction factors

Figure 2.3 shows that the peak stress increases as the percentage of attachment area increases. For the cases studied, the friction factor does not seem to produce a significant difference in peak stress, this difference is only 0.87% at the lowest percentage of ILT attachment area (0%). If we compare the extreme cases (0% and 100%), there is a difference of approximately 3.5% between the peak stresses. From these results, it can be concluded that ILT with incomplete attachment areas in combination with low friction factor values exert lower stress on AAA walls.

The peak stress values assuming a friction factor of 0.1 are plotted again in Fig. 2.4,

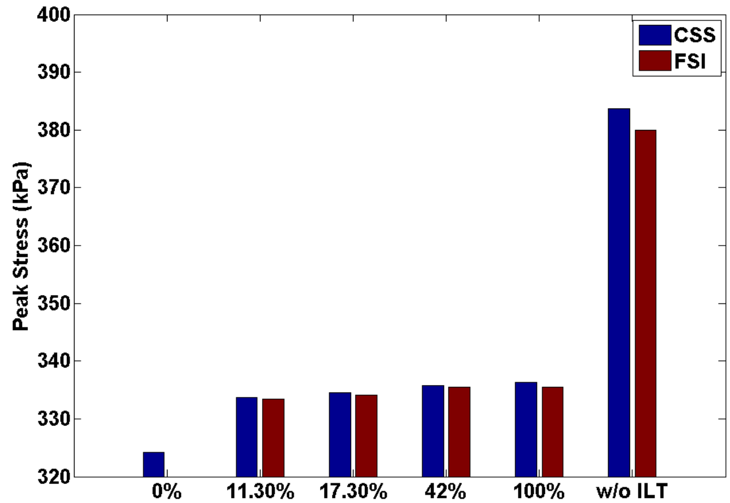

Figure 2.4: Maximum aortic wall stress for different ILT attachment areas. The 0% configuration corresponds to and ILT held in place only by friction.

which also includes a case without ILT (aneurysm alone) for comparison purposes. A considerable reduction in the peak stress is observed when ILT structures are present on AAAs. There is 14.8% difference in the peak stress for an aneurysm without ILT and for the fully detached configuration (CSS simulation). This suggests that the presence of ILTs could reduce the risk of rupture of AAA walls as also pointed out by Di Martino in a similar work [15]. In addition, the effect of incomplete attachment areas is not harmful to the AAA wall because it does not promote a significant increase in the peak stress. Of course, these preliminary results are predicated upon the assumed attachment types and profiles, which have not included the modelling of cracks in the ILT structures, which could expose certain regions of the AAA wall to the full flow pressure while other regions of the wall are protected by the ILT. In addition, both CSS and FSI simulation results are included in Fig. 2.4 for comparison purposes. No significant differences were found between CSS and FSI analysis, and our results were found to be consistent with those reported in previous work that focused on calculating the impact of arterial compliance on the AAA wall stress [59].

To expand the discussion, a study was performed using another hypothetical, asymmetric 3D AAA geometry. Three cases were simulated in this analysis finding peak stress values of 364.11, 333.80, and 334.08 kPa for the AAA without ILT, partially detached ILT, and fully attached ILT, respectively. Figure 2.5 shows the graphical representation of stress distribution for two of the cases. There is approximately an 8% of difference of peak stress values between the artery alone and incompletely attached case, supporting our previous results and analysis. From Fig. 2.5, it is possible to observe that the stress distribution on the AAA wall is smoothed by the presence of ILT structures, see Fig. 2.5 (b).

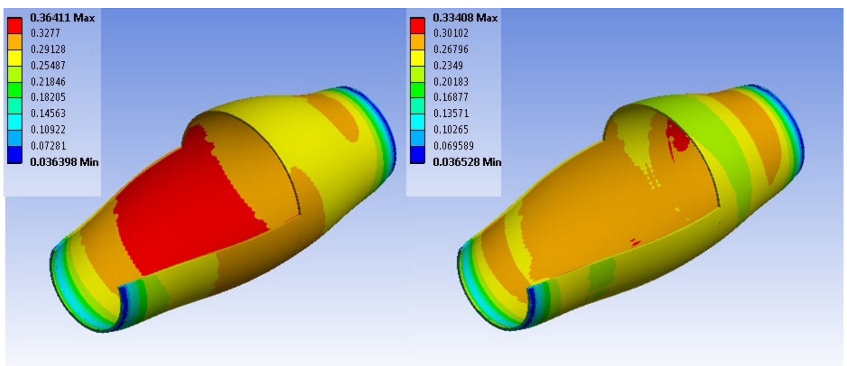

(a) (b)

Figure 2.5: Stress distribution of an asymmetric 3D AAA. (a): AAA without ILT, (b): AAA including ILT full attachment.

The results obtained suggest that ILT structures play a protective role on AAAs from the mechanical point of view. It is important to point out that the lower peak stresses were found in cases of fully detached ILTs that exert contact forces on the wall through a friction factor. However, since a uniform pressure along the luminal surface was applied in this case, tangential forces were neglected, and these could potentially dislodge fully detached, friction-held ILTs. The FSI simulations results showed that the inclusion of tangential forces as consequence of the constant volumetric flow imposed at the inlet of the system did not caused significant changes on the peak stress compared to the same cases but simulated under uniform luminal pressure conditions (CSS). This finding agree with the common knowledge pointed out in other researches that the internal pressure is perhaps the main influence on the AAA wall rupture. To obtain more conclusive results, more comprehensive studies are needed including realistic flow environments, e.g., under pulsatile blood flows conditions. Results from the proposed work may have an impact in practice as tools for design/re-design of endovascular devices that promote ILT formation, as knowledge-base for evaluating their effectiveness in AAA repair, and to formulate model-based guidelines both for elective repair and for site-specific deployment of such devices.

Chapter 3

Modelling of Porous Stents for AAA Repair

3.1 Introduction

After verifying that incomplete ILT attachment to the AAA wall does not increase the stresses acting on it, we now proceed to the modelling fluid flow through the porous stents. This is in compass with the main objectives proposed in this thesis research project, which is to increase our understanding of blood flow promoted by porous stents and the finding of optimal stent configurations to efficiently protect AAA walls from hemodynamic flow forces. Thus, this chapter is focused on simulating the flow through porous stents under different conditions. Based on the results of these detailed simulations, we will estimate model parameters that will allow us to later simulate the porous stent with a lower computational cost. In Chapter 4, these models with lower computational cost will be used to conduct simulations on idealized aneurysm geometries with and without porous stents, allowing us to study the impact of the stent on the hemodynamic conditions inside the AAA sac. In the next chapter, these parameters are implemented into the commercial software ANSYS-CFX to perform simulation on an idealized aneurysm geometry with and without stent to study their impacts on the hemodynamic factors inside the aneurysm sac.

3.2 Methodologies for Modeling Porous Media

3.2.1 Immersed Medium Method (IMM)

The IMM considers the details of the cavities inside the porous media where the fluid passes through. The void volumes of the media have to be appropriately meshed in order to improve convergence and numerical stability. For instance, in our project, we are interested in studying the impact that porous stents have on the flow inside aneurysm models. To this aim, appropriate meshing schemes are needed to capture hemodynamics factors accurately. But, due to the enormous difference in size between the cavities of the porous media and the endovascular system, typically from the continuation of the thoracic aorta to the iliac arteries, a prohibitive number of elements would need to be employed to obtain reliable results. To solve this issue, a porous media model (PMM) could be employed to reduce computational time and become an alternative.

3.2.2 Porous Media Model (PMM)

The PMM is a suitable method to overcome the expensive computational resources required to obtain results from CFD simulation of multilayer stents in AAAs. The porous media can be modelled using Forchheimer law, which implicitly captures the relevant flow parameters,

$$0 = \frac{\partial p}{\partial x_i} - \frac{\mu}{\kappa} u_i - C \rho u_i \left| u \right| \tag{3.1}$$

where μ is the viscosity of the fluid, κ the permeability and C the Forchheimer's coefficient. Equation 3.1 can be arranged as a quadratic polynomial of the velocity as shown in Eq. 3.2. The parameters a and b represent the inertial and viscous flow effects, respectively.

$$\Delta p = au^2 + bu \tag{3.2}$$

where $a = \frac{1}{2}C\rho\Delta e$, $b = \frac{\mu}{\kappa}\Delta e$, with Δe being the thickness of the porous media and ρ the density of the fluid. These coefficients can be calculated from experimental data (if available) or, as in this work, from CFD simulations. Thus, we can use them to model the pressure drop effect through stents without needing the excessive number of mesh cells around the struts of multilayer stents. This information is employed to model the presence of multilayer stents by scaling the terms on the Navier-Stokes equation using a symmetric area porosity tensor K and the porosity associated with the local position of the cell along the stent domain. The pressure drop effect is included into the source term of the discretized equation of motion and scaled with the corresponding vector area available to flow trough an infinitesimal planar control surface.

3.3 Methodology

To develop a computational modelling approach that efficiently considers the multiple length scales that are relevant for fluid flow phenomena in AAAs treated with porous stents, CFD simulations are carried out with the ANSYS commercial software. These simulations were run on a small region of the stent taking advantage of symmetry and periodicity, and ignoring boundary effects at the stent edges. The calculation of these detailed simulations will allow us to study the porous media and estimate its permeability, flow resistance among other parameters to represent the stent as a porous media of known properties, thus being able to model the hemodynamic effects of the porous stent at a reasonable level of accuracy but with a lower computational cost. It is important to mention that in this work we restricted the degrees of freedom of the stent pores by keeping the relative position of the struts constant. In other words, we only considered changes of stent porosity caused by changes in the wide-screen angle. However, this is no way limits the applicability of the proposed approach. Additional CFD studies could be conducted to determine the effect of other design changes on the parameters that capture the hydrodynamic behavior of the stent.

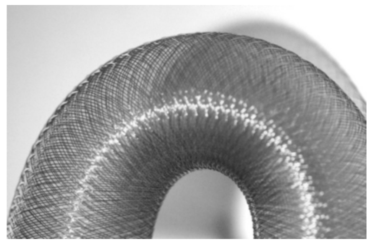

Figure 3.1: The multilayer stent. Picture taken from Sultan et. al [66]

From Fig.3.1, we can observe that the cavities of the porous stent resemble a rhombic shape if we extend the cylindrical surface in a plane. By assuming this shape, we can perform simulation on small domains of the stent, see Fig. 3.2, to obtain pressure drop and other hemodynamic factors of interest to perform studies on AAAs treated with multilayer stents.

To start evaluating the impact of the stent structure on the pressure drop, the following parameters for a single layer stent are varied: stent porosity, the parameters defining the mid-angle of the rhombic element or screen-wide angle α, and the angle of incidence of the flow β defined with respect to a normal unit vector on the stent surface. The CAD model used for this approach is shown in Fig. 3.2, which simulation domain is used to study the interaction between the flow and the spacial configuration of stents. For instance, the angle of incidence β is equal to zero when the stent is aligned with the vertical global axis (Y), i.e, when the flow is normal to the stent wall. An uniform velocity and zero gauge pressure are set at the inlet and outlet borders respectively and symmetry conditions on the lateral faces. Then, varying the inlet velocity in the physiological range, curves of pressure drop for different parameters can be obtained.

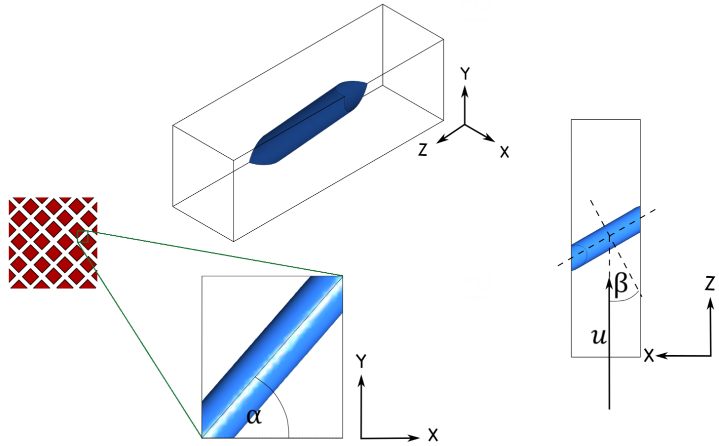

Figure 3.2: Schematic representation of the simulation domain needed to perform CFD studies. The flow direction is modelled by varying the angle of incidence β, and the stent porosity is function of the wide-screen angle α.

3.4 Convergence Study

To ensure a correct calculation of the hemodynamic parameters through the stent pores, a gradual increase on the number of cells is performed. The number of cells is incremented using a sphere of influence method that varies the density of the elements toward the stent struts where high velocity gradients appear. The mesh used consisted of tetrahedral and prism elements distributed around the stent strut as shown in Fig. 3.3.

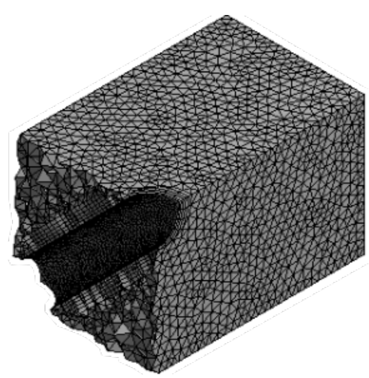

Figure 3.3: Mesh distribution around a circular strut of the stent in a quarter of the pore domain

Convergence was obtained using a residual criteria of $1 \cdot 10^{-05}$ for improving accuracy and achieving asympthotic behavior of the hemodynamic parameters of interest. A mesh-sensitivity analysis was performed using the stent configuration case of highest velocity gradients, lowest possible angle of incidence β and highest wide-screen angle α. The study determined a maximum face sizing element size of $9.5 \cdot 10^{-07}$ m which led to approximately 600,000 cells within a simulation domain with a total volume of $2.9332 \cdot 10^{+06}$ μ m^3. By this mean, the obtained coefficients of the pressure drop are reliable and can be employed to model the presence of the stent at a lower computational cost in comparison to other porous medium model methodologies.

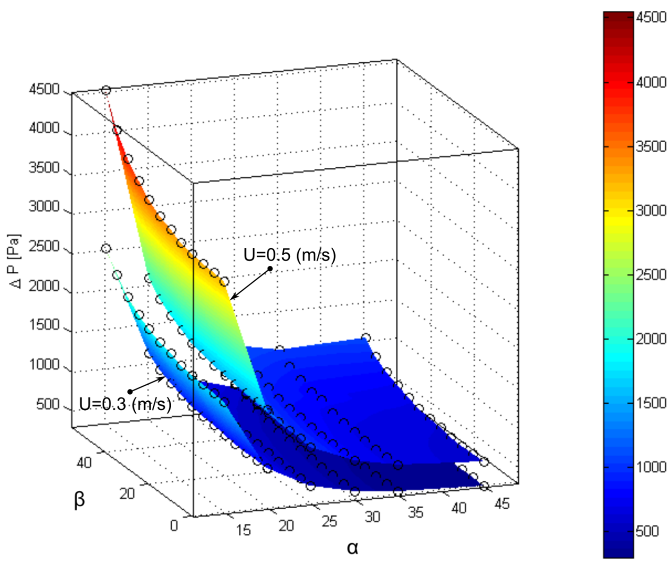

Figure 3.4: Pressure drop curves for different wide-screen angles and angles of incidence in the range of $\alpha = 15° - 45°$ and $\beta = 0° - 45°$.

The results obtained indicated that the pressure drop increases at high angle of incidence β and low wide-screen angle α. This pattern can be observed from the pressure drop curves plotted in Fig. 3.4 where two physiological flow velocities are shown (0.3 and 0.5 (m/s)). Note that for wide-screen angles below 25° the pressure drop increases drastically having a more preponderant role on the flow resistance that the angle of incidence. It can also be noted that the pressure drop curves are almost parallel in all part, except at the highest angles of incidence (flow almost tangent to the stent).

In summary, the PPM methodology was able to capture the hemodynamic parameters of interest for different stent configurations and flow velocities. We noted that the pressure through the stent increases as the angle of incidence increases and the wide-screen angle decreases. These results can be used to model the presence of the stent under a low computational cost instead of using an IMM that consider all the details of the porous media. As mentioned in section 3.3, the relative position of the stent struts was kept constant, limiting our study to a range of pore sizes controlled by the wide-screen angle. In case of furthering the study to other geometric factors, additional CFD simulations are needed to capture the corresponding model coefficients.

3.5 Cases of Study

To understand the effect of the stent porosity on the hemodynamic factors inside the AAA sac, a hypothetical 2D axisymetric AAA geometry, shown in Fig.3.5, is used to perform simulations with and without the stent. The geometrical factors used to build the AAA were taken from previous studies conducted by Finol *et al.* [21].

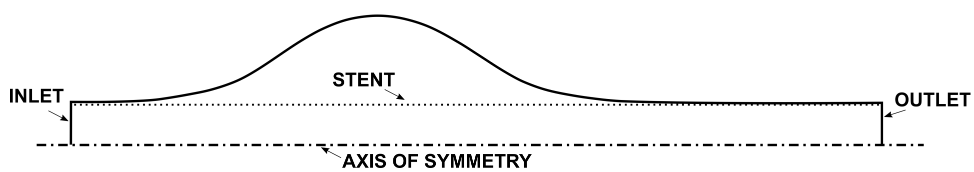

Figure 3.5: Axisymetric 2D AAA geometry with the porous stent

Two flow conditions are studied in this section. A steady-state simulation applying a parabolic velocity profile and a periodic state governed by a pulsatile velocity. The cardiac pulse is modelled by applying a physiological wave form at the inlet of the AAA domain. This velocity is the peak systolic velocity reached in the physiologic abdominal aorta velocity waveform reported by Morris *et al.* [41]. Thus, a velocity inlet condition can be imposed as a function of time and the radius of the artery at the inlet expressed as follow,

$$u(r,t) = \left[\frac{a_0}{2} + \sum_{i=1}^{n} (a_i sin(i\omega t) + b_i cos(i\omega t)) \right] * f(r) \tag{3.3}$$

where a_0, a_i, b_i are coefficients of the Fourier series and $f(r)$ is a function, quadratic for instance, used to shape the velocity profile of the blood. Figure 3.6 shows the fitted curve of the wave form employed in this study.

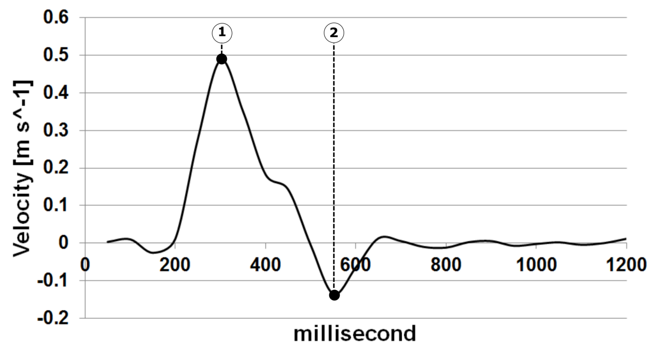

Figure 3.6: Velocity waveform at the inlet of the AAA, [41] marked with two stages chosen for plotting the hemodynamic field of interest.

3.6 Mesh independence study

Mesh resolution tests and convergence studies were performed for cases with and without stent. For the case without stent, hexahedral and tetrahedral meshes with prismatic elements on the aneurysm wall were employed to understand their benefits in terms of calculation time and accuracy of results. Global and local mesh controls allow us to vary the mesh size and distribution in the aneurysm domain for mesh convergence analysis, employing the maximum value of the pressure and the shear stress on the AAA wall as parameters to monitor convergence towards mesh-independence. We found asymptotic behaviours on the parameters at $79,256$ mesh elements for the case using the tetrahedral mesh as indicated in Fig. 3.7 and $11,799$ elements for the hexahedral mesh. In order to ensure the accuracy of results, the shear strain rate was monitored at the distal end of the aneurysm for systematic mesh refinements. The results show no significant fluctuation on this variable between two consecutive mesh refinements beyond those required for mesh-independent estimation of pressure and shear stress on the aneurysm wall. For the cases with stent, a combination of hexahedral and tetrahedral elements was employed, with especial refinement at the proximal and distal points of the AAA sac. The porous domain that models the presence of the multilayer stent was set with hexahedral layers of 4 elements on the radial direction in order to model the pressure drop across the stent. Mesh convergence required more elements than the case without stent , mainly because of the small stent thickness and large flow gradients across and in the vicinity of the stent.

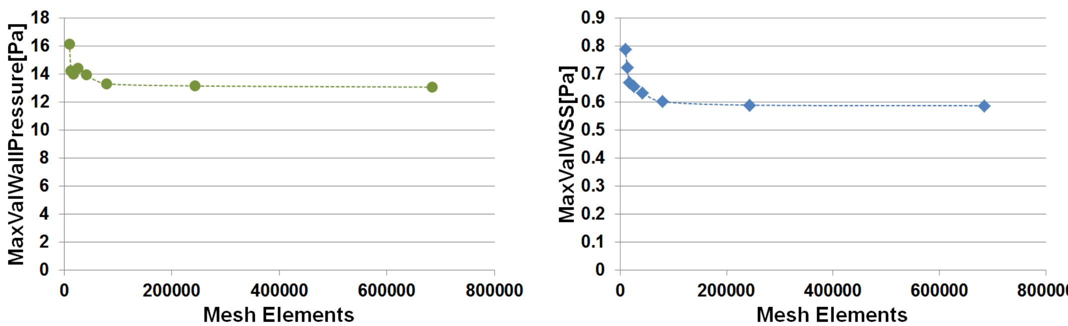

Figure 3.7: Pressure and WSS maximum value behaviour on the AAA wall for consecutive mesh refinements

3.7 Steady-State Results

In order to understand the blood flow changes caused by the stent, in this section we present plots of pressure, velocity, shear strain rate distribution, and streamlines for the AAA with and without the stent in Figs. 3.8, 3.9 and 3.10, respectively. The cases including the stent, Figs. 3.9 and 3.10, were set with a porosity value of 0.698 and 0.455 which correspond to wide-screen angles α equal to 45° and 15° respectively. It is important to mention that the simulations were run keeping constant the angle of incidence at different levels, without observing significant changes on the overall results. Thus, the angle of incidence β was kept constant in all cases (45°).

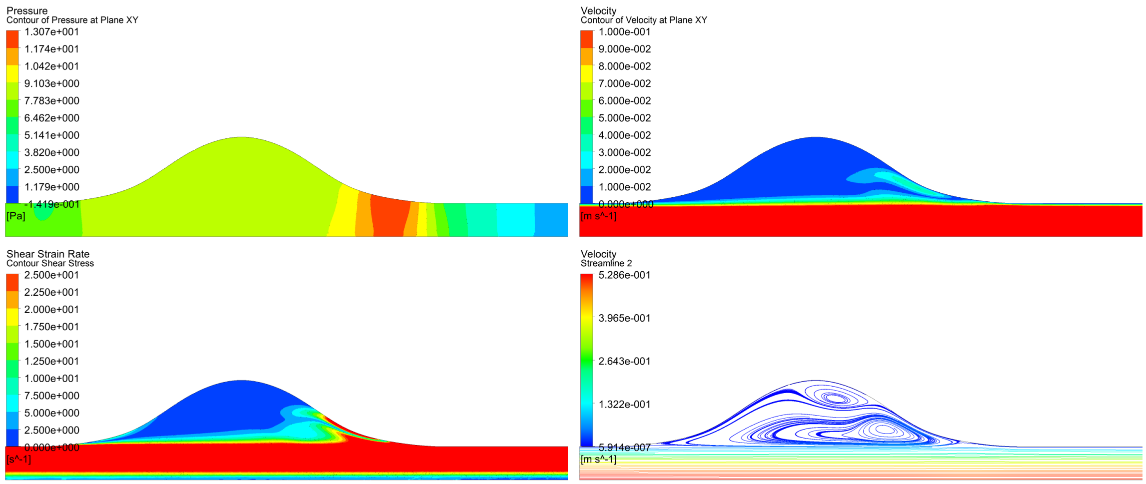

Figure 3.8: Contours of pressure, velocity, shear strain rate and streamlines distribution for the AAA without stent

Comparing the resulting streamlines shown in Fig. 3.8 and Figs. 3.9 and 3.10, we can notice that the presence of the stent reduces the convective acceleration effect on the fluid reducing the chance of flow separation, characteristic observed in the AAA case without stent shown in Fig. 3.8. In other words, the stent increases flow resistance, damping flow instabilities found during regime of flow transition (laminar-turbulent transition), avoiding flow separation and vortex formation inside the AAA sac. As consequence, the velocities, the pressure and the shear strain rate distribution inside the aneurysm sac are reduced, decreasing the intensity of the hemodynamic forces acting on the AAA wall. An approximate reduction of 18.9% and 67.4% on the maximum values of the dynamic pressure and shear stress on the AAA wall was observed when comparing the case of wide-screen angle equal to $\alpha = 45°$ and the case without stent. Table 3.1 shows results for different wide-screen angles, observing an increase of the dynamic pressure and decrease of the WSS while the porosity of the stent decrease.

To support our observations, we evaluated the effect of the stent on the radial velocity entering the aneurysm sac. A control line on the stent, parallel to the axial axis, was set to observe the changes on the radial component of the velocity entering the sac shown in Fig. 3.11. From this plot, we can observe how the stent reduces the velocity and

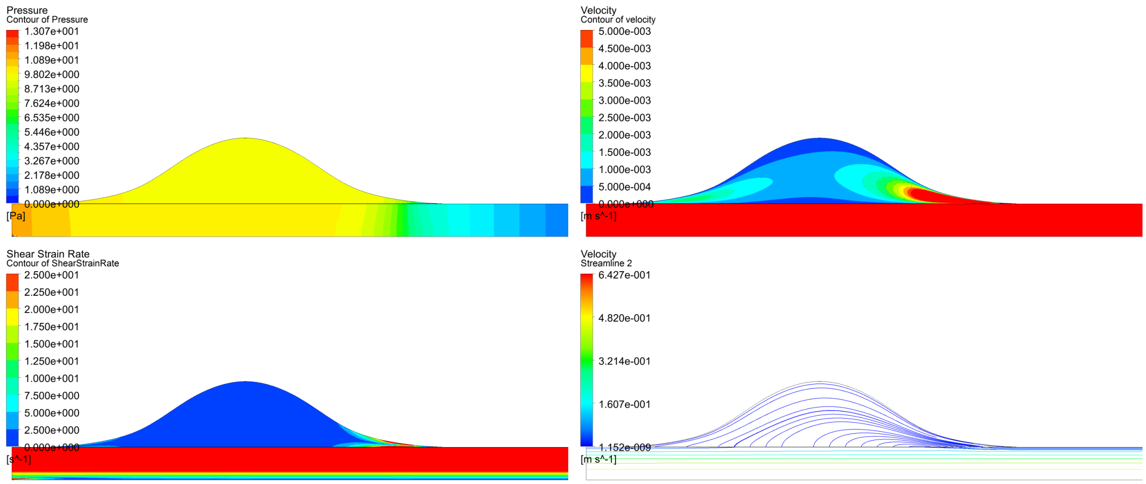

Figure 3.9: Contours of pressure, velocity, shear strain rate and streamlines distribution for the AAA with stent set with a uniform wide-screen angle equal to 45°

the convective acceleration term on the radial direction, specifically the rate in which the radial velocity change with respect to the axial axis of the system $\frac{\partial v_r}{\partial x}$, changing the flow pattern inside the AAA sac. Besides, it is noticed the existence of a point where the radial velocity changes in direction with respect to the control line. This point appears on different positions of the stent depending to the stent porosity configuration, modifying the mode of action of the stent on the flow, i.e, changing the flow resistance distribution along the stent that lead to changes on the hemodynamic parameters on the AAA wall. For instance, in this case study we observe that this point moves proximally as the stent porosity decreases, increasing the maximum value of the shear stress attained by the aneurysm wall. It is observed that the shear stress on the AAA wall was reduced the most when this point lies closest to the center of the stent. This is a consequence of the resistance of the stent which control the areas where the volumetric blood flow enters and exits the aneurysm sac through the stent.

Consequently, we proceeded to vary the local properties of the stent to observe changes on the maximum pressure and WSS. Table 3.1 shows results for different uniform porous distribution ($\alpha = 45°, 30°, 15°, 10°$) to understand its effect on the hemodynamic factors inside the AAA sac.

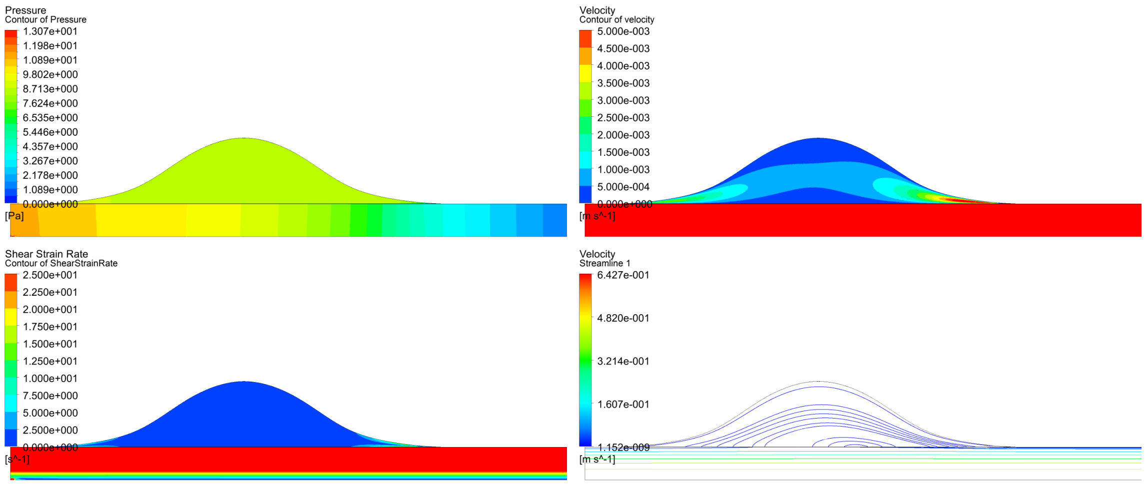

Figure 3.10: Contours of pressure, velocity, shear strain rate and streamlines distribution for the AAA with stent set with a uniform wide-screen angle equal to 15°

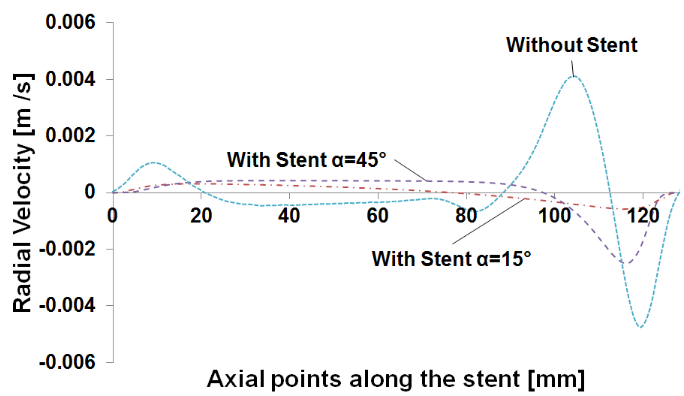

Figure 3.11: Radial velocity distribution along the control line on the surface of the stent for the AAA with and without the stent

In addition, to understand the effect of non-uniform stent porosity distributions, we performed simulations varying the local porosity of the device using the porosity distributions shown in Fig. 3.12, given by the equations below,

$$VP_1(x) = -1.0 \cdot 10^{-4}x^2 + 7.0 \cdot 10^{-17}x + 0.7045 \tag{3.4}$$

$$\begin{aligned} VP_2(x) = & -1.0 \cdot 10^{-11}x^6 + 7.0 \cdot 10^{-19}x^5 + 6.0 \cdot 10^{-8}x^4 \\ & -4.0 \cdot 10^{-15}x^3 + 4.0 \cdot 10^{-05}x^2 + 3.0 \cdot 10^{-12}x \\ & + 0.2846 \end{aligned} \tag{3.5}$$

Table 3.1: Maximum pressure and WSS for cases without and with stent of wide-screen angles $\alpha : 45°, 30°, 15°, 10°$ and uniform-porosity distribution

Cases	MaxWSS [Pa]	MaxPressure [Pa]
Without Stent	0.586	13.06
With Stent, $\alpha = 45°$	0.191	10.58
With Stent, $\alpha = 30°$	0.180	10.58
With Stent, $\alpha = 15°$	0.096	10.73
With Stent, $\alpha = 10°$	0.099	10.86

Table 3.2: Maximum values of pressure and WSS under different porosity distributions

Cases	MaxWSS [Pa]	MaxPressure [Pa]
VP_1	0.052	10.68
VP_2	0.134	10.65

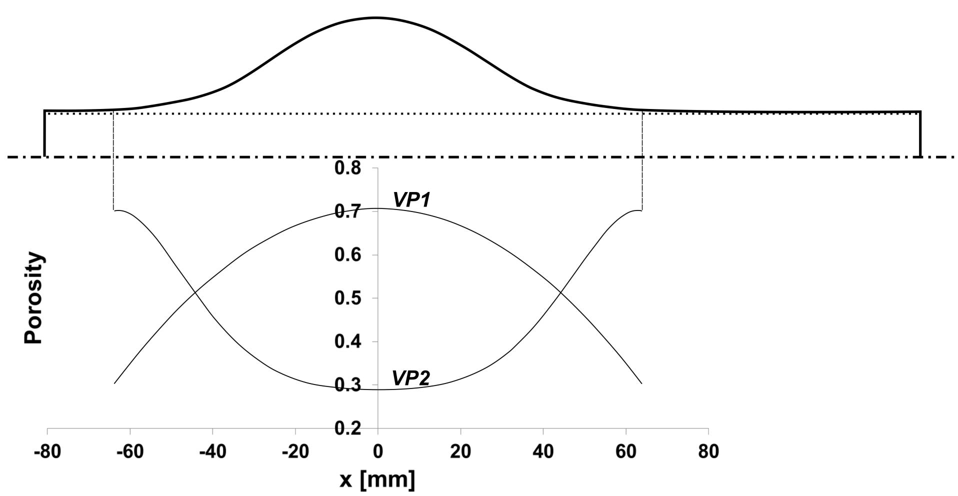

Figure 3.12: Porosity functions along the stent

Function VP_1 represents a case when the porosity of the stent is lower at the distal and proximal zones of the AAA and higher values at the center, while the function VP_2 models the opposite. Tables 3.2 shows the maximum values of the pressure and shear stress on the AAA wall for these two cases.

The two porosity distributions examined in this section showed changes on all the hemodynamic parameters of interest inside the sac, Fig. 3.13 and Fig. 3.14. Notably, the WSS was more reduced with the stent configuration VP_1 due to the highest flow resistance opposed at the proximal end of the stent in comparison to the stent configuration VP_2 which allows faster flow at the distal zone of the AAA wall.

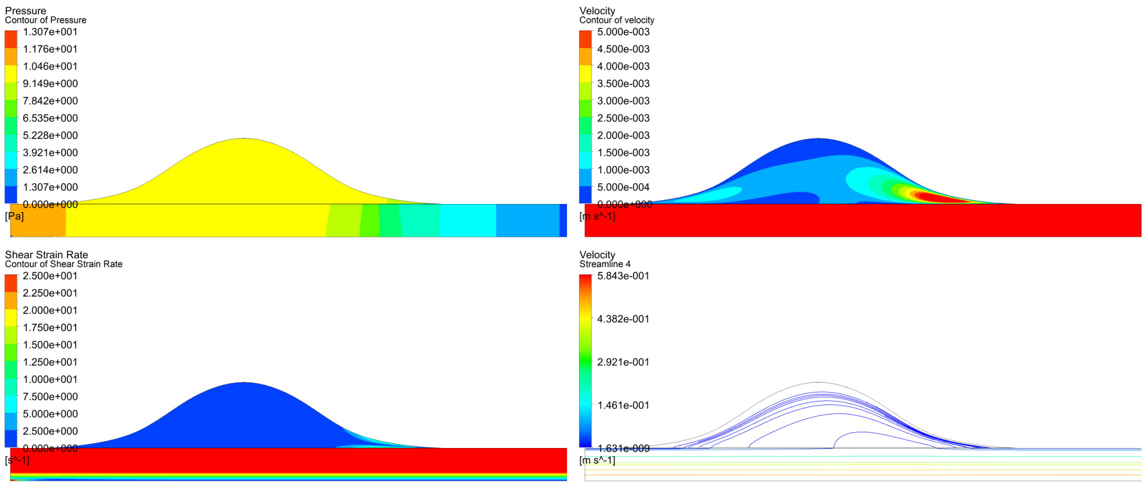

Figure 3.13: Contour of pressure, velocity, shear strain rate and streamlines under the porous distribution VP_1

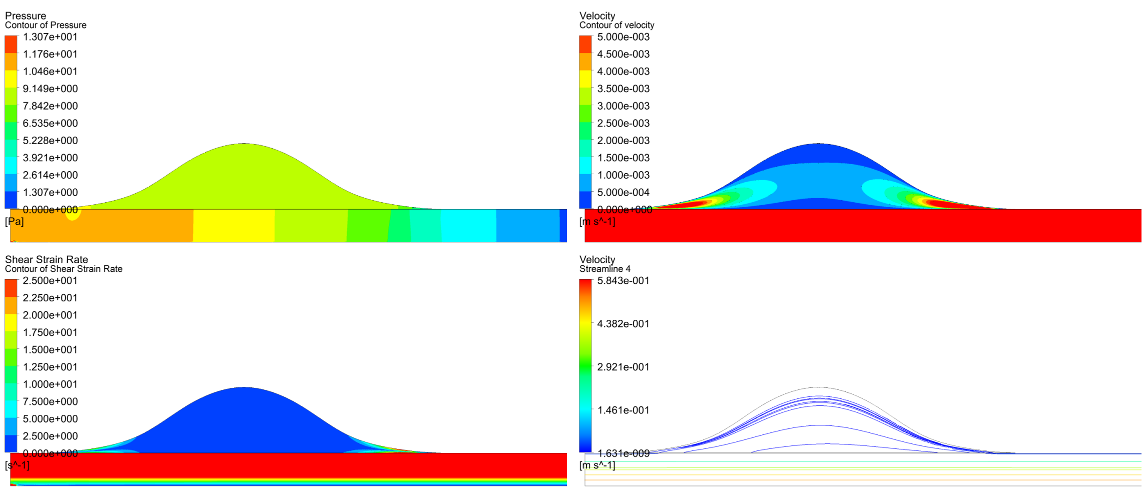

Figure 3.14: Contour of pressure, velocity, shear strain rate and streamlines under the porous distribution VP_2

It is important to mention that the implementation of the effect of the wide-screen angle is easier and computationally more convenient than the implementation of the angle of incidence because it sets up the porosity and that is a parameter of the porous media model. In any case, because the stent is tangential to the main flow, we assumed an isotropic flow resistance, and assigned the values that correspond to $\beta = 45^o$. This

Table 3.3: Maximum pressure and WSS for cases without and with stent set with porous distribution VP_1 and VP_2 at systolic peak

Cases	MaxWSS [Pa]	MaxPressure [Pa]
Without Stent	1.66	443.62
With Stent (VP_1)	1.65	575.05
With Stent (VP_2)	3.61	594.76

Table 3.4: Area average values of pressure and WSS for cases without and with stent set with porous distribution VP_1 and VP_2 at systolic peak

Cases	AveWSS [Pa]	AvePressure [Pa]
Without Stent	0.30	339.39
With Stent (VP_1)	0.28	405.12
With Stent (VP_2)	0.50	416.90

assumption did not affect the results, for instance, a maximum of 6% on the maximum WSS value was observed comparing results using an angle of incidence $\beta = 20^o$ and $\beta = 45^o$.

3.8 Transient Results

To model a pulsatile blood flow condition, we apply a physiologically relevant velocity wave at the inlet of the AAA domain. The velocity profile is assumed parabolic in the cross-section of the blood vessel, with its peak velocity changing in time according to the waveform represented in Fig. 3.6.

To solve the governing equations, CFD simulations performed in the ANSYS-CFX software were carried out, using a second order Euler transient scheme. The time step size was set equal to 0.008125 seconds, leading to 136 time steps per cardiac cycle. A total of four cycles were performed to obtain the steady-periodic solution, only the results from the last cycle are shown here. A Root Mean Square (RMS) residual criteria of $1.0 \cdot 10^{-4}$ was set for the governing equations.

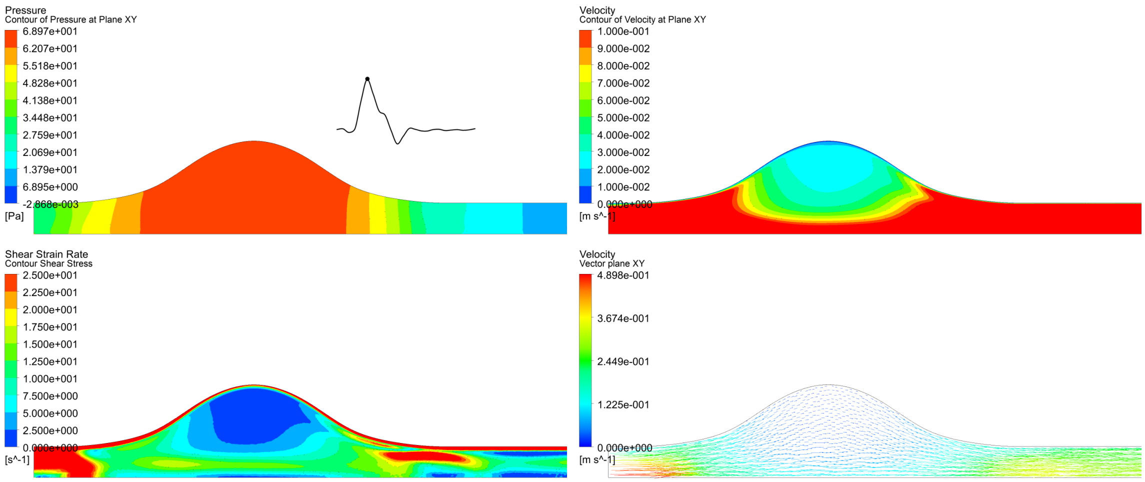

Figure 3.15: Contour of pressure, velocity, shear strain rate and vector of velocity for the AAA without stent at stage 1

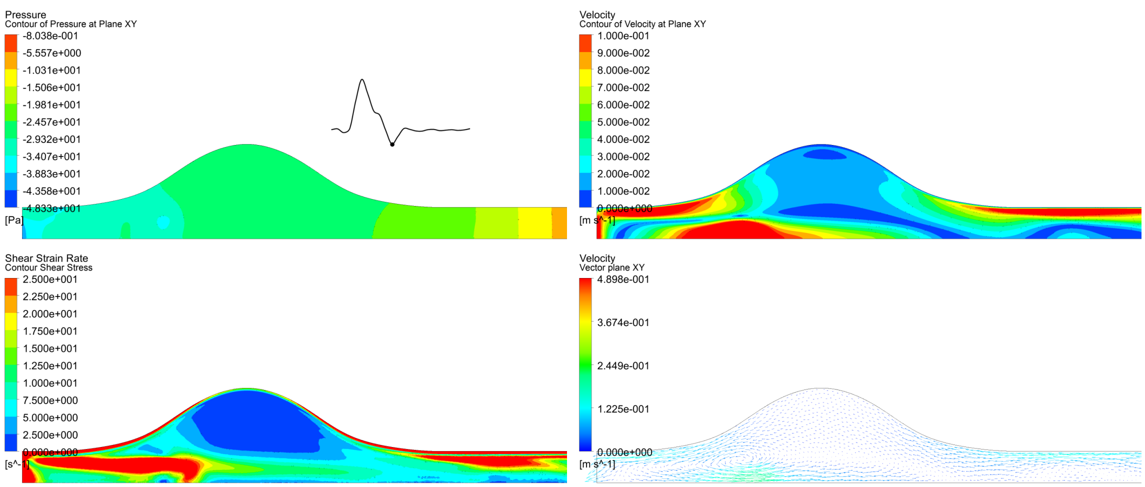

Figure 3.16: Contour of pressure, velocity, shear strain rate and vector of velocity for the AAA without stent at stage 2

Figures 3.15-3.16, and Figs. 3.17-3.18, show the results for cases without and with stent, respectively. The case with stent was set with the VP_1 porous function shown in Fig. 3.12. Tables 3.3 and 3.4 show the maximum and average values of the pressure and shear stress on the AAA wall for cases with and without stent during one cardiac cycle. These results show that the presence of the stent set with the VP_2 porosity distribution increases the maximum and average values of the pressure and shear stress on the AAA wall in approximately 34.06% and 22.8%, and 117.4% and 66.6% with respect

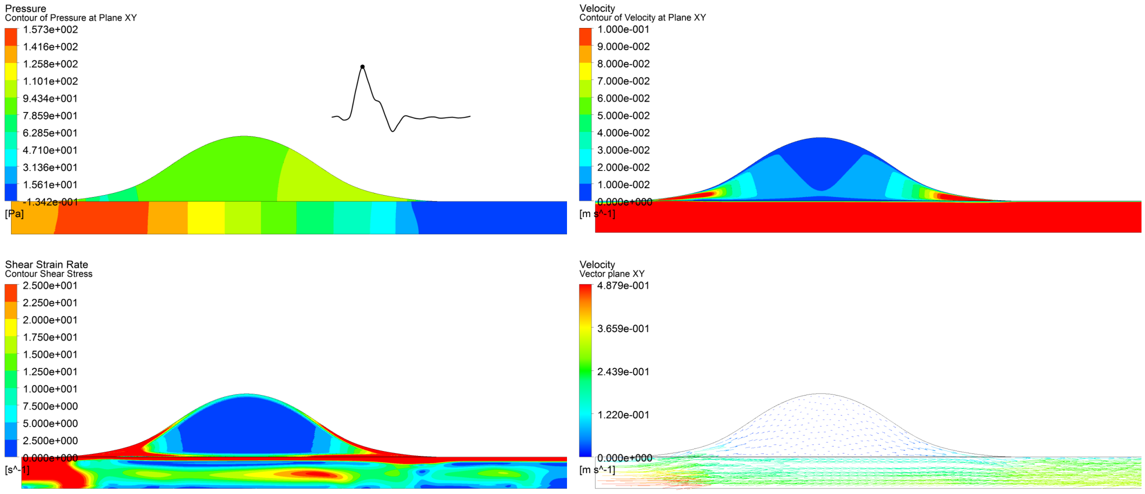

Figure 3.17: Contour of pressure, velocity, shear strain rate and vector of velocity for the AAA with stent under a porous distribution VP_2 at stage 1

to the case without stent. These differences are reduced by changing the stent with a porous distribution VP_1 in approximately 29.62% and 19.36% for the maximum and area averaged values of the pressure. However, the maximum and area averaged shear stress are 0.6% and 6.66% lower with respect to the case without stent.

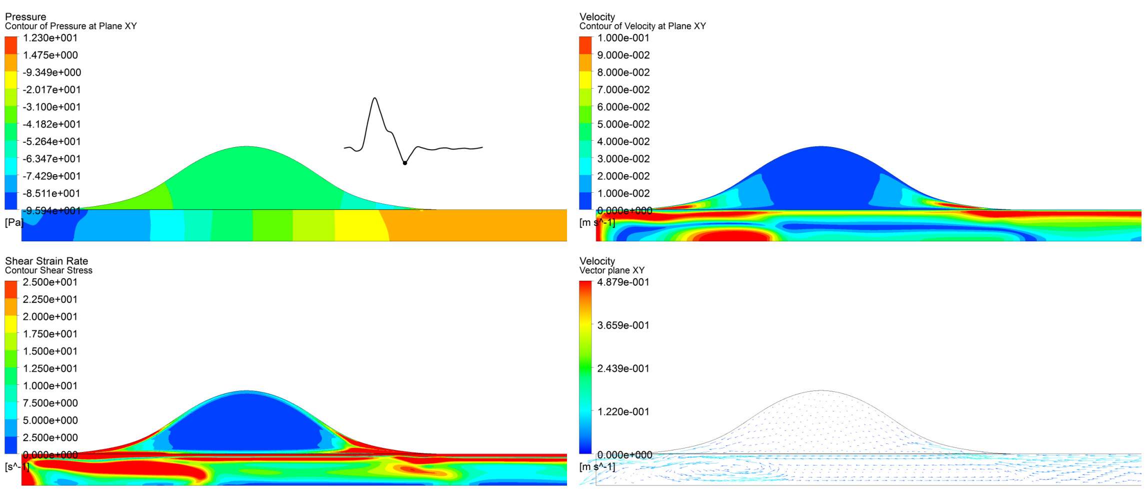

Figure 3.18: Contour of pressure, velocity, shear strain rate and vector of velocity for the AAA with stent under a porous distribution VP_2 at stage 2

In summary, under steady-state condition, the presence of the stent reduces the velocity inside the aneurysm sac, and the maximum values of the pressure and WSS compared with the case of aneurysms without stent. Also flow recirculations were reduced when the stent was present, however, for the wide-screen angle equal to 10°, we observed recirculation areas inside the aneurysm sac. We hypothesize that this phenomenon is caused by stent of uniform porosity distribution and the small wide-screen angle which increases the flow resistance specifically at the distal zone where the blood flow exits the aneurysm sac. The stent cases set with local variation of porosity showed similar values of maximum pressure but a difference of 61.1% on the maximum values of the WSS. Regarding to transient simulations, we noted that the inertial effect of the flow caused significant changes on the parameters of interest inside the AAA sac compared to results obtained under steady-state flow conditions. Interestedly, we observed that any stent porosity configuration does not ensure the reduction of the WSS inside the sac. Only the VP_1 stent porosity case was able to reduce the average WSS inside the sac at systolic peak compared to the AAA case that did not consider the presence of the stent.

3.9 Conclusions

A study of stent flow resistance was successfully done for a layer of stent with the pore size found in multilayer stents used for EVAR of AAAs. The method makes it possible to determine the pressure drop in a stent layer varying its geometric properties. The pressure drop model were used to set constant and local variation of the stent porosity to understand the hemodynamic impacts inside the AAA sac. Under steady-state conditions, the presence of the stent decreases the velocity of the blood flow entering the sac, reducing disturbances and the maximum values of the pressure and shear stress on the AAA wall according to the porosity distribution of the stent. However, results from transient simulations showed that the pressure increased with the two stent configurations used in this section and only one of them reduced the shear stress inside the AAA sac. However, this rise on pressure, observed during the systolic phase of the pulsatile flow, should not be of concern because it represents no more than 2% of increase with respect to the total pressure inside the AAA sac. From these results, we can conclude that the hemodynamic factors inside the AAA sac are increased or reduced depending on the stent configuration which is difficult to predict prior the AAA reparation. To avoid inappropriate hemodynamic behavior inside the AAA sac as consequence of the stent porosity, a methodology to design porosity distributions for targeting hemodynamic safe parameters inside the sac is needed to avoid the increase of AAA wall rupture risk and to systematise the finding of a proper stent configuration regardless the flow, side branches and shape of AAAs.

Chapter 4

Design Methodology

4.1 Design Methodology for Porous Stents

The purpose of this design methodology is to find stent porosity distributions that induce hemodynamic environments useful for reducing the progression of the aneurysm without increasing the risk of rupture. In general terms, porous stents reduce the flow into the aneurysms, minimize the arterial damage caused by turbulent structures, reduce the blood flow recirculation, laminarize the blood into the parent vessel smoothing the wall shear stress distribution inside the sac, and allow the patency of blood to renal and other vital branches. However, these flow characteristics might not be enough to ensure an efficient hemodynamic control inside the aneurysm sac, causing unsuitable hemodynamic scenarios if the stent configuration is arbitrarily chosen. Works in the literature have shown superior outcomes from EVAR using porous devices in comparison to procedures using traditional and fenestrated stent grafts [2, 25, 47, 67]. For instance, a study on 14 patients conducted by Henry *et al.* [25], reported no periprocedural complications, branch patency of 100%, progressive sac thrombosis and shrinkage, and mortality of 0% after 36 months of follow up, whereas fenestrated endovascular repair has showed a higher mortality of 25% at 36 months [54]. Despite this promising evidence, there are reported cases in which patients have suffered complications [30, 36]. Lazaris *et al.* [30] reported a case where the patient died 12 months after device implantation. The authors concluded that the probable cause of the failure was related to the porosity of the device. Another recent follow-up by Lowe *et al.* [36], reported three cases of death occurring within a 12-month post-surgery period. One patient died perioperatively, the second post-surgery but without evidence of aneurysm growth, and the third with evidence of 9 mm growth in the AAA diameter with respect to its pre-surgical dimension.

In order to improve outcomes and reduce post-operative complications, we study how the stent design affect blood circulation patterns inside the AAA sac. We hypothesize that patient-specific porous stents can be designed to achieve optimal hemodynamic conditions inside the AAA sac. Currently, there are no tools available for this task. In this chapter, we leverage the simulation models discussed in Chapter 3 to formulate a methodology to determine a suitable porous stent configuration to achieve a target hemodynamic environment. The following hemodynamic parameters will be employed for this aim: a) pressure on the AAA sac, b) shear stress on the AAA wall, and c) mass flow into the sac at peak systole. These three parameters have been chosen because they provide useful information related to the susceptibility of the aneurysm wall to rupture and the hemodynamic environment influencing intraluminal thrombus formation. There is a range of porosity distributions that could induce the target range of the hemodynamic parameters, and with the help of the proposed methodology we will be able to find suitable stent configurations that prevent undesirable blood flow conditions inside the AAA sac leading to arterial mechanical failure.

In the previous chapter we used different stent configurations to observe the changes in the blood flow inside the AAA sac, finding inappropriate hemodynamic behaviors in some cases. Thus, in order to avoid inappropriate hemodynamic scenarios, we formulate a methodology using the simulation models that we have priorly developed, which represent the presence of the stent as a porous medium with known pressure drop characteristics, to determine a set of porosity distributions that result in favorable hemodynamic conditions. The range of hemodynamic conditions inside the AAA sac used for this task will be taken from the existing literature and will be considered as an external input to the design methodology.

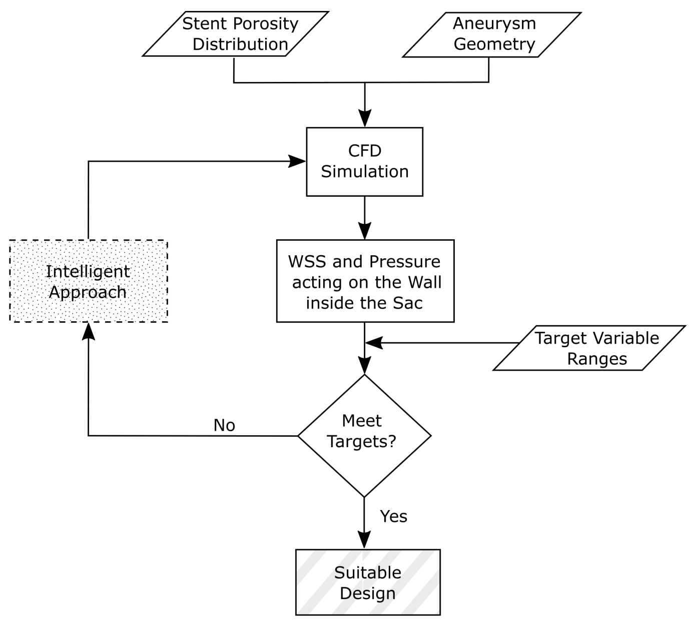

Figure 4.1: Simulation workflow for finding porosity distributions that induce safe hemodynamic conditions inside the AAA sac.

Figure 4.1 is a schematic representation of the proposed design methodology. The target variable ranges discussed in the next section are sets of hemodynamic parameter values that define what is considered a safe environment to slow or prevent AAA growth and wall rupture. If a porosity distribution is found to induce these hemodynamic parameters, a suitable design has been found. If not, we will use an intelligent approach to generate candidate porosity distributions until an appropriate porosity distribution inducing the hemodynamic requirements is found.

4.2 Target Ranges for Hemodynamic Parameters

The progression of aneurysms is a multifactorial problem that involves phenomena across multiple length scales. It could be triggered due to metabolic disorders that impact the quality of the AAA wall material properties leading to the enlargement of the artery that in turn alters the flow behavior of the blood. From a macroscale fluid perspective, the interplay between hemodynamic factors (such as wall shear stress (WSS), pressure) and vascular remodelling has not been completely elucidated in the scientific literature. However, a few works have identified hemodynamic scenarios that could be disadvantageous for the integrity of the AAA wall. For instance, Boyd *et al.* [6] recently showed, rather counter-intuitively, that low shear stresses and low pressures are better predictors of the location of AAA wall rupture than high shear stress and/or pressure. In their work, the researchers conducted steady-state blood flow simulations in 7 patient-specific geometries of ruptured AAA (rAAAs). Their results showed that AAA wall rupture occurred in zones of low velocity and most cases in areas of blood recirculation, where low shear stress and ILT formation is predominant. On the other hand, Xenos *et al.* [88] studied ruptured AAAs under more realistic conditions. In their research, the authors performed fluid-structure interaction simulations on patient-specific geometries under pulsatile blood flow, reporting values of pressure and WSS for ruptured AAAs cases and a normal abdominal aorta. From these works, we can infer that there is a range of hemodynamic conditions that reduces the risk of AAA wall rupture. Table 4.1 summarizes these results that would be used to define plausible hemodynamic ranges.

Table 4.1: Hemodynamic values taken from Xenos *et al.* work [88].

Subject	P_{sys} (mm Hg)	ΔP_{sys} (mm Hg)	WSS_{sys}^{max} (Pa)	WSS_{sys}^{min} (Pa)
ruptured AAA_1	122.5	2.1	0.30	0.06
ruptured AAA_2	122.8	2.4	0.27	0.05
normal abdominal aorta	120.4	0	2.40	0.9

To prevent the progression and rupture of AAAs, a porous stent device should promote a suitable hemodynamic environment inside the sac, e.g., within the aforementioned hemodynamic ranges. These ranges of flow parameters are shown in Table 4.2, where $\tau_{avg,sys}$, ΔP, and $\dot{m}_{sac}$ represent, respectively, the spatially averaged wall shear stress, the spatially averaged pressure acting on the AAA wall at peak systole, relative to the baseline case without stent, and the mass flow through the stent. These ranges have been defined from the information presented in a host of publications, including [4, 6, 88]. It is important to mention that the behavior of the endothelial cells depends mostly on the WSS. Specifically, low WSS in combination with a prolonged flow circulation of biological particles could degenerate the adventitia, potentially increasing the risk of AAA wall rupture [1, 7, 28]. Therefore, the flow resistance of the stent should be designed to promote flow conditions that reduce the recirculation patterns inside the AAA sac and the WSS gradients along the AAA wall to restrict high rates of intraluminal thrombus formation [6, 12].

Table 4.2: Target ranges for hemodynamic parameters for pulsatile conditions.

$\tau_{avg,sys}$ (Pa)	ΔP (Pa)	$\dot{m}_{sac}$ (l/min)
0.9-2.4	Minimize	$\dot{m}_{sac} > 0.0$

4.2.1 Wall Shear Stress

From experimental and computational works studying the connection between AAA progression and hemodynamic changes inside the AAA sac [57], it has been observed that the enlargement of the AAA causes a reduction in WSS. The increase in AAA volume also decreases the intensity of the vortex rings that appear after peak systole. In connection, other researchers have reported that rapid formation of ILT is prevalent at zones of high WSS gradients [6]. For illustration, Fig 4.2 shows the flow streamlines, indicating the points in the AAA wall with the highest WSS gradients; note that their location changes during the cardiac cycle, Fig. 4.3. This causes an unbalanced ILT growth that impacts the integrity of the aneurysm wall and increases the chances of AAA wall rupture, due to the proteolytic degradation in the wall segments covered by thicker ILT structures [6, 68].

4.2.2 Pressure

The pressure on the AAA wall has been linked to aneurysm rupture [16], so it is a critical hemodynamic parameter that needs to be considered for the design of the porous stent. In contrast with impermeable stents that divert the flow away from the aneurysm walls thus eliminating the pressure acting on it, porous stents act as flow regulators and, as such, modify the pressure distribution on the aneurysm wall but do not eliminate it. Figure 4.4 compares the pressure distribution acting on the AAA wall with and without stent at peak systole. Note that the effect of the porous stent is to decrease the pressure in some regions while increasing the pressure almost anywhere else in the aneurysm wall. Figure 4.6 compares the average pressure acting on the aneurysm wall, for cases with and without stent of different porosity distributions (VP_1, VP_2, VP_3, VP_4) illustrated in Fig. 4.5. Once again, the overall effect of the stent is to increase the average pressure, a trade-off for the ability to regulate the flow into the aneurysm sac. Hence, the porosity distribution of the stent should be designed in a way that minimizes the increase of pressure (ΔP) with respect to a baseline. For the purpose of the proposed methodology, the baseline pressure will be determined from simulations in the AAA without a stent, hence $\Delta P = P_{avg,stented} - P_{avg,baseline}$.

4.2.3 Mass Flow

The principle of operation of the porous stent is to regulate the blood flow into the aneurysm sac. This can only be achieved if the stent is indeed porous, i.e., if there is blood flow across the porous stent into the sac. The magnitude of this mass flow, although related to the flow velocity, pressure, shear stress and other flow characteristics, has not been documented in the reviewed literature. Instead, the literature has focused

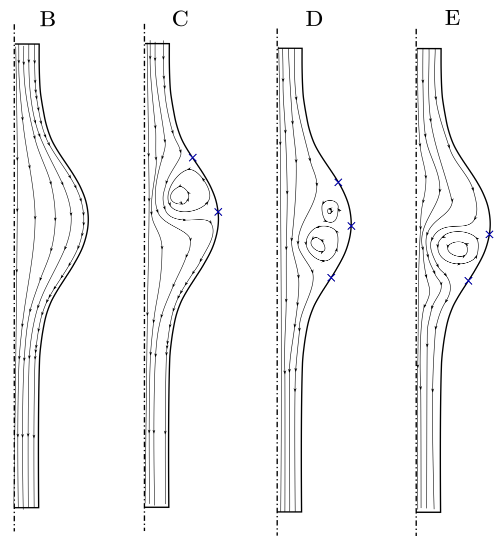

Figure 4.2: Blood flow through an AAA at different times of the cardiac cycle.

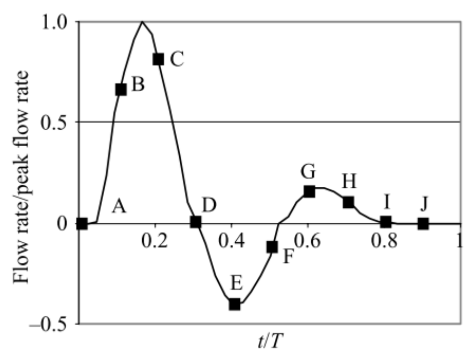

Figure 4.3: Volumetric flow for one cardiac circle commonly found in AAAs [57].

on shear stress, pressure and velocity as primary parameters of interest. This preclude us from establishing an evidence-based target range for the blood flow into the sac. Instead, we must rely on ensuring the blood flows across the porous stent indirectly through a target value for the minimum shear stress in the aneurysm wall. Enforcing a minimum value of WSS on the AAA wall during peak systole indirectly implies that, at any point inside the aneurysm during peak systole, there will be flow through the porous stent towards the aneurysm sac following the general direction of the main flow. In addition, the formulation of the intelligent approach for the design of the porous stent, discussed in the next section, will include an inequality constraint to ensure non-zero flow into the aneurysm sac, which can also be constrained indirectly by defining a non zero lower

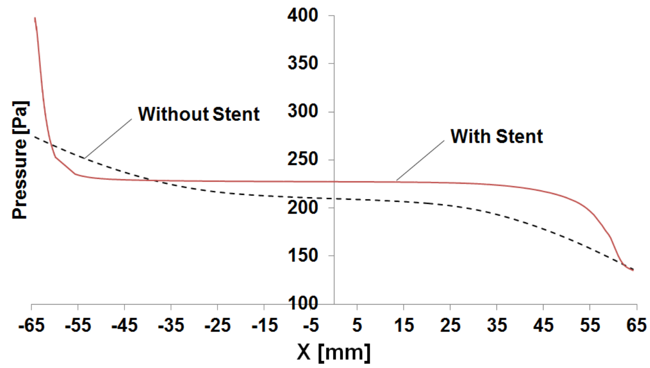

Figure 4.4: Pressure distribution on the AAA wall at peak systole with and without stent.

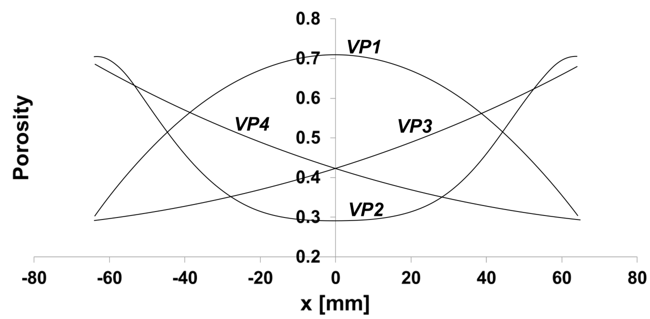

Figure 4.5: Porosity functions

bounder in the WSS range.

4.3 Intelligent Approach

The next step in the proposed design methodology is the specification of an algorithm for finding suitable porosity distributions that ensure safe hemodynamic conditions inside the AAA sac. The design objectives are to ensure that the WSS inside the AAA sac at peak systole is within the range indicated in Table 4.2, that the increase in pressure caused by the stent is minimized, and to ensure that there is blood flow into the AAA sac through the porous stent. To achieve these design objectives, the porosity distribution of the stent will be used as the design variable.

Let us define the porosity distribution as a dimensionless mathematical function

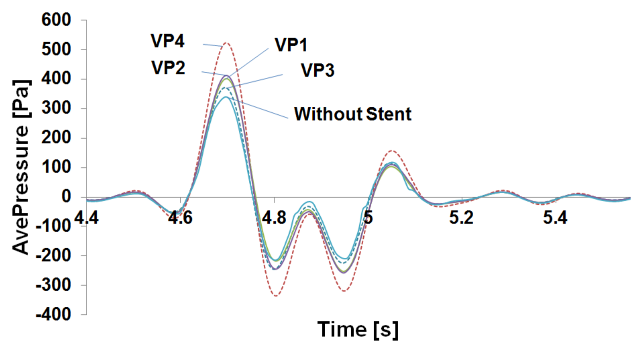

Figure 4.6: Average pressure on the AAA wall during one cardiac cycle, [62].

$S(x^*)$, representing the porosity of the stent at any given point x^* over its length with $0 \leq S(x^*) \leq 1$ for all x^*. The dimensionless length $x^* = \dfrac{x}{L}$ represent the ratio between the coordinate position of a point along the stent with respect to a system of reference and its total length $2L$. For simplicity in the nomenclature, we have dropped the asterisk to point out the dimensionless form of the variables. To formulate the problem, we will parameterize the porosity distribution $S(x)$ as a cubic spline, using a small number of control points to represent the porosity along the stent. Splines are piecewise-polynomials defined over an interval of real variables $[a, b]$, composed of k subintervals $[x_i, x_{i+1}]$ with

$$a = x_1 < x_2 ... < x_k < x_{k+1} = b$$

Using splines, the porosity distribution $S(x)$ over the i-th interval $[x_i, x_{i+1}]$ is defined to be the polynomial $P_i(x)$, $x \in [x_i, x_{i+1}]$ so that

$$S(x) = \begin{cases} P_1(x), & \text{for } x_1 \leq x < x_2 \\ P_2(x), & \text{for } x_2 \leq x < x_3 \\ \vdots & \\ S(x) = P_{k+1}(x), & \text{for } x_k \leq x < x_{k+1} \end{cases} \tag{4.1}$$

The polynomials $P_i(x)$ used in this work are third-order polynomials, their coefficients determined such that the first and second derivatives of $S(x)$ are continuous at each nodal point $[x_i]$. Under this approach, the curve $S(x)$ is parameterized by the coordinates of the nodal points x_i, also called knots, and by $S_i = S(x_i)$, the value of the porosity distribution at each nodal point i, with $i = 1, \ldots, n_{knots}$. In our particular case and for illustration purposes, we will consider $n_{knots} = 5$ uniformly distributed points along the length of the stent, i.e., $x_i \in [-1, +1]$, for the stent considered in our simulations cases, with a length of $2L = 128.4$ mm. By considering the knot points as uniformly distributed, we remove from consideration 5 design variables, namely the location of the know points along the length of the stent. Hence, this leaves $S_1, \ldots, S_5$ as the only parameters defining the shape of the porosity distribution, Fig. 4.7.

The parameterization of the porosity distribution described above allows us to formulate the design problem mathematically in terms of a small set of design variables, namely the value of the porosity S_i at the nodes x_i, $i = 1, \ldots, 5$. In addition, this parameterization based on polynomial splines ensures the porosity distribution is (mathematically) smooth, which is beneficial for convergence and stability of the simulations. More importantly, the parameterization allows us to represent a wide range of porosity distributions with just a few parameters, thus representing the design space of all porosity distributions efficiently. Finally, this parameterization allows us to easily impose constraints on the parameters $(S_1, \ldots, S_5)$ so that the values of the porosity are physically meaningful at any point along the stent, that is, $0 \leq S(x) \leq 1$ for all x, where $S = 0$ corresponds to an impermeable point on the stent and $S = 1$ to a fully permeable point. In summary, the chosen parameterization efficiently covers the design space while ensuring enough degrees of freedom to consider many porosity distributions, guarantees smoothness of the porosity distribution for simulation purposes, and implicitly constraints porosity values to the physically meaningful range. Based on this parameterization of the porosity distribution, the proposed approach will change the vector of parameters $\vec{\mathbf{S}} = (S_1, \ldots, S_5)$ to modify the porosity distribution so that deviations of the flow parameters from their

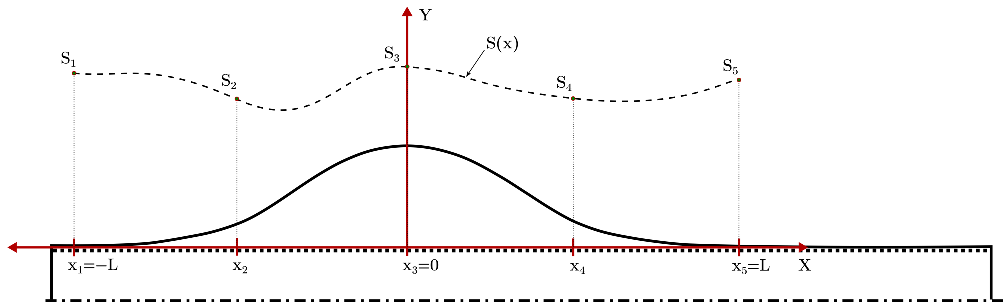

Figure 4.7: Spline parametric curve schematic representation of a stent positioned at the entrance of the AAA sac.

target ranges are minimized. Let $\tau(x,t)$ be the shear stress at time t at point x inside the aneurysm sac, and $\Delta P(x,t)$ be the increase of pressure at point x and time t with respect to the AAA without a stent. Let $\tau_{avg,sys}$ be the spatially averaged wall shear stress inside the sac at peak systole, and $\Delta P_{avg,sys}$ be the spatially averaged pressure acting on the AAA wall at peak systole, relative to the baseline case without stent. Then, the mathematical formulation of the proposed intelligent approach is the optimization problem:

$$\min_{\vec{\mathbf{s}}} \sum \left([\Delta P]^2\right) \tag{4.2}$$

subject to

$$\tau_{avg,sys} \leq WSS_{sys}^{max} \tag{4.3a}$$

$$\tau_{avg,sys} \geq WSS_{sys}^{min} \tag{4.3b}$$

$$\dot{m}_{sac,sys} > 0.0 \tag{4.3c}$$

$$0 \leq S_i \leq 0.7, i = 0, \ldots, 4 \tag{4.3d}$$

The first two constraints, (4.3a) and (4.3b), ensure that the average shear stress inside the aneurysm sac at peak systole is within the target range as per Table 4.2. Constraint

(4.3c) ensures that there is blood flow into the sac through the porous stent at peak systole, while constraint (4.3d) limits the design variables, i.e., the porosity at each of the nodal points, to lie on a range that guarantees that the resulting porosity distribution S(x) is physically meaningful at any point x in the stent. Note that an alternative formulation of this optimization problem could substitute constraints (4.3a) and (4.3b) so that, instead of enforcing the target WSS range based on spatial averages, it would be enforced at any point inside the aneurysm sac. Such a formulation would require one constraint for each nodal point in the computational grid used for the CFD simulation, thus increasing the complexity of the optimization problem significantly. Hence, we have decided for the formulation shown above as a trade-off between accuracy and computational tractability.

4.3.1 Implementation

The workflow in Fig. 4.8 shows in detail the implementation of the optimization process for finding suitable porous stent designs. In particular, we are interested in controlling the WSS and pressure inside the AAA wall. The iteration process starts with a given AAA geometry and an initial porous distribution for the stent; these are set into the ANSYS-CFX software used to numerically solve the differential equations that govern the flow phenomena. Once solved the equations of motion, the WSS and pressure along the AAA wall are compared to specific target values. If the flow field predicted by the simulation matches the target values, the loop stops and reports the suitable porosity distribution found. If not, the process continues to the next step, where a new porosity distribution is determined by the iterative step of the optimization algorithm. Then, the new porosity distribution is written into a text file, which is used to update the simulation setup that is passed on to ANSYS-CFX to run the new simulation. The process continues until the objective function is minimized while satisfying the optimization constraints.

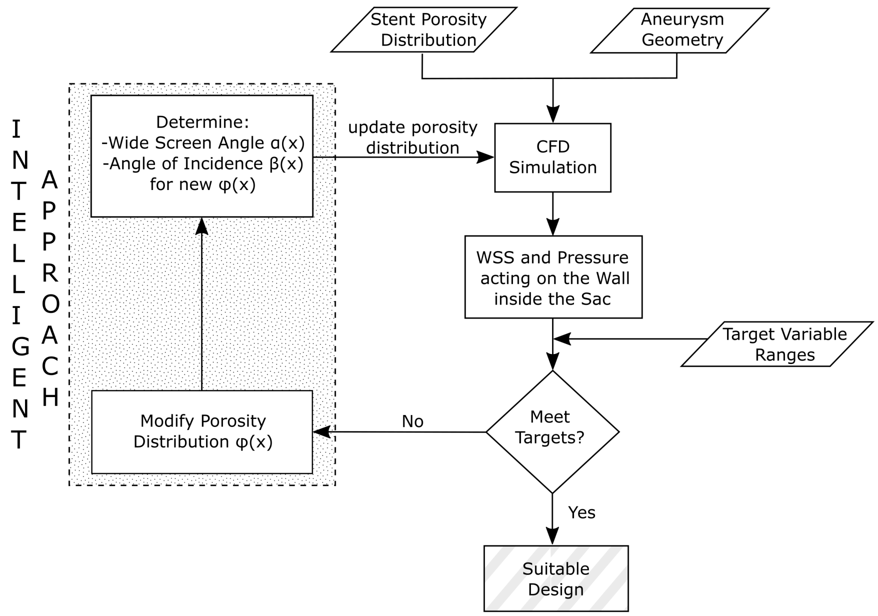

Figure 4.8: Implementation of the optimization methodology.

4.3.2 Optimization Under Steady-State Flow Conditions

To test the proposed design methodology, a steady-state study was conducted. Many works have modelled AAA flow as steady-state [6, 92]. The assumption of steady-state reduces the computational cost and time required for the proposed study, yet it allows us to demonstrate the capabilities of the methodology without loss of generality. The ranges in Table 4.2 were formulated based on the literature but they were extracted from transient studies. Thus, a new hemodynamic target range was defined for the present steady-state studies. In the proposed methodology, the target ranges for the hemodynamic parameters are considered as input, to be provided by the medical team, so herein we define a target range only for illustrating the capabilities of the methodology. In particular, to define the range shown in Table 4.3 we considered that, in steady-state, the contribution of inertial forces to the shear stress at the AAA wall is less significant, so the resulting shear stresses would be lower than those calculated under transient conditions. In addition, we considered the shear stress field of the baseline case without stent as a reference. Hence, the shear stress range shown in Table 4.3 represents a considerable reduction with respect to this baseline case, yet it is expected to be attainable by the methodology.

Table 4.3: Target ranges of hemodynamic parameters for steady-state conditions.

τ_{avg} (Pa)	ΔP (Pa)	$\dot{m}_{sac}$ (l/min)
0.001-0.005	Minimize	$\dot{m}_{sac} > 0.0$

4.4 Results

4.4.1 Sensitivity Study

To understand the impact of the stent porosity on the hemodynamic changes inside the AAA sac, we carried out sensitivity analyses using five Uniform Porosity Distributions (UPDs) increasing monotonically their stent porosity values: 0.31, 0.4, 0.5, 0.6, 0.67.

Figures. 4.9 and 4.10 show the resulting streamlines, isovelocity contours, WSS, and radial velocity across the stent corresponding to the five UPD cases. It is observed that the WSS and the radial velocity across the stent increase as the porosity of the stent increases. Changes on the isovelocity contours are observed for stent porosity values higher than 0.5. Note that at low porosity levels the flow patterns are similar, specifically cases i) and ii) in Fig. 4.9. At higher porosity values, cases iii), iv), and v) in Figs. 4.9 and 4.10 respectively, flow speed and pattern differences are more notorious. Interestingly, a vortex appears in all cases regardless of the stent porosity as consequence of the dominant effect of the viscous forces inside the AAA sac. Note also that radial velocity distribution exhibits rapidly fluctuating veolcities at the proximal and distal ends of the stent. This behavior is an artifact of the mesh discretization, mainly due to the cell sizes and transition between mesh zones and element types. Although the magnitude of these artifacts could be reduced by a finer discretization, we considered the simulation results shown in Figs. 4.9 sufficient for our main purpose, i.e., illustrating the suitability of proposed methodology for simulation-based design of porous stents for EVAR.

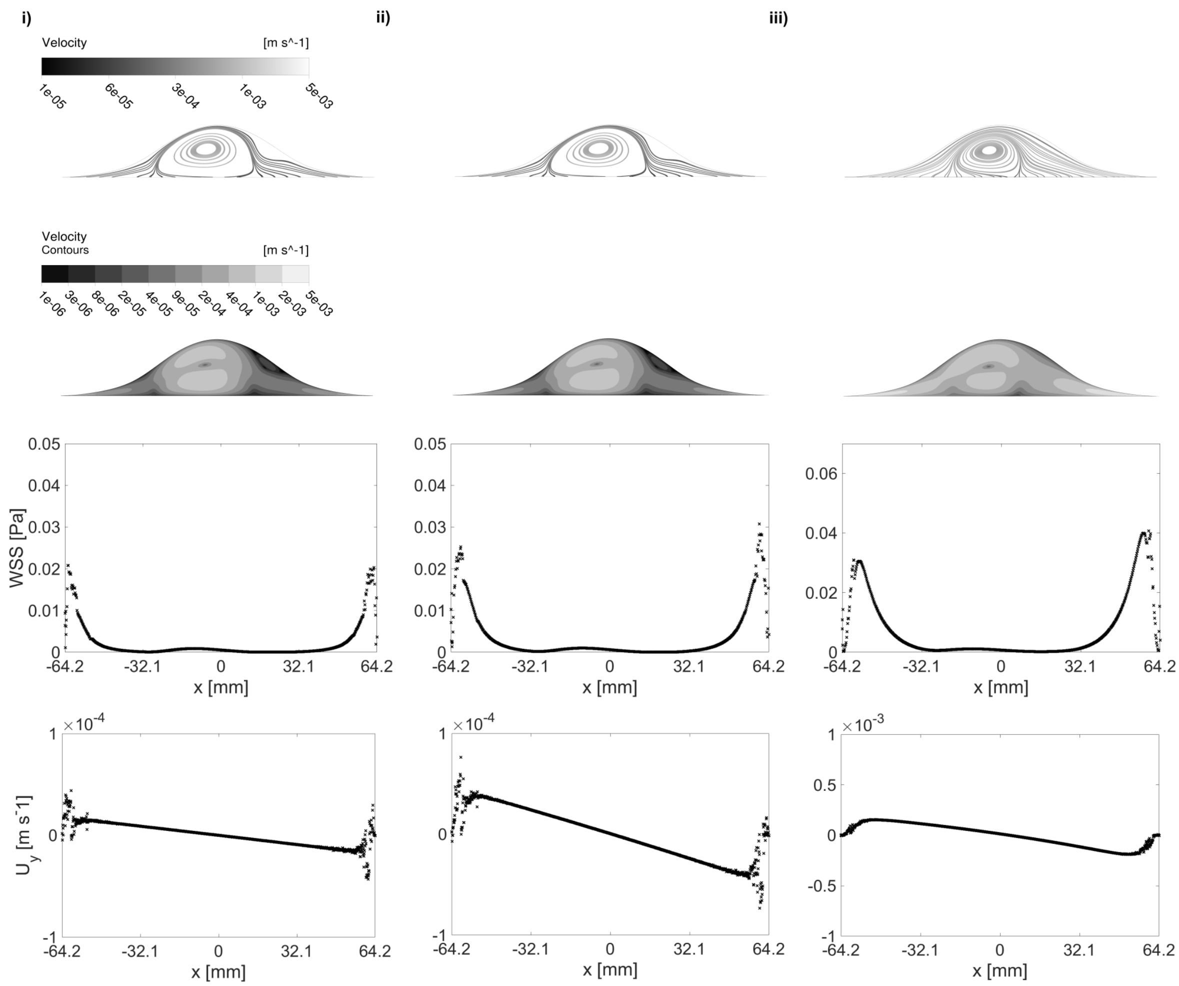

Figure 4.9: Streamlines, isovelocity contours, WSS, and radial velocity across the stent plots corresponding to the solution obtained using the porous settings: i)UPD$_1$=0.31, ii) UPD$_2$=0.4, iii) UPD$_3$=0.5.

To complement this sensitivity study, two additional non-uniform stent cases were simulated, shown in Fig. 4.11. These cases correspond to stents with the Porosity Increasing Toward Distal (PITD) and the Porosity Decreasing Toward Distal (PDTD) configurations, referred to as VP_3 and VP_4 in Fig. 4.5, respectively. Results from these stent configuration cases are presented in Fig. 4.12. We can observe that the streamlines, the isovelocity contours, and the velocities across the stent follow similar but mirrored patterns. For instance, the streamlines are very similar if we mirror one of the streamline patterns with respect to a vertical line situated at x=0 mm, a point where the porosity

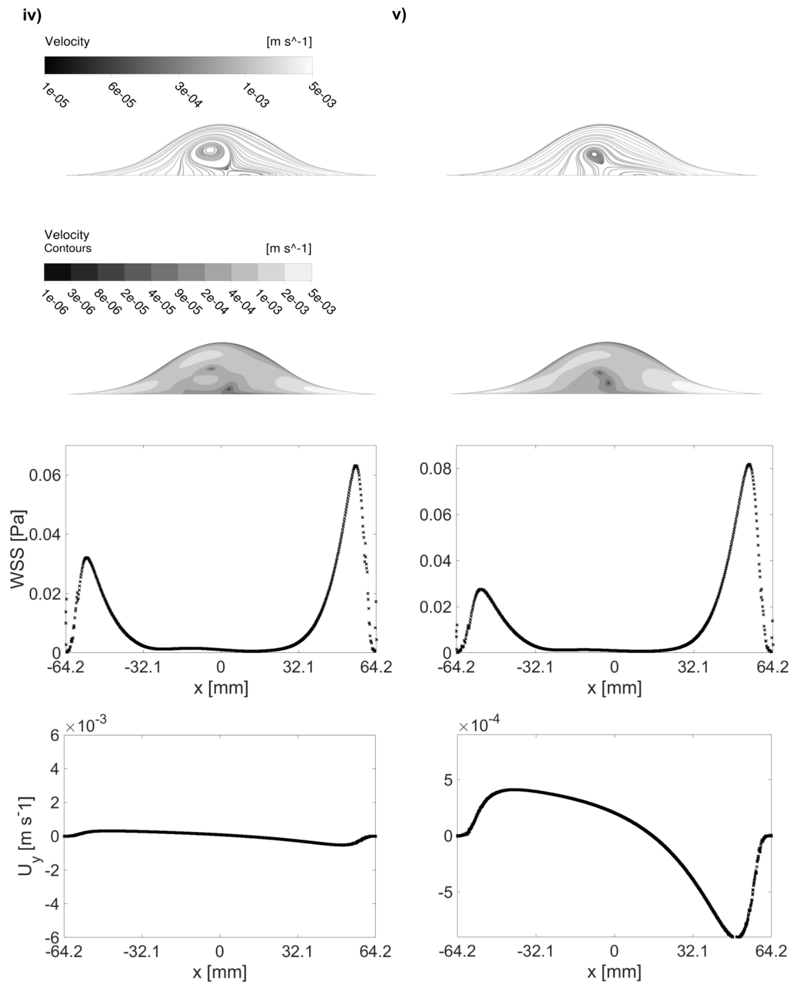

Figure 4.10: Streamlines, isovelocity contours, WSS, and radial velocity across the stent plots corresponding to the solution obtained using the porous settings: iv)UPD$_4$=0.6, v) UPD$_5$=0.67.

in both stent configurations has the same value. In the same fashion, the trends in the distribution of radial velocity across the stent are similar but mirrored with respect to a vertical line at x=0 mm and with respect to the flow direction. Notably, the point in which the radial velocity changes in direction, which depends on the stent porosity configuration, differs in both cases, affecting the hemodynamic parameters inside the AAA sac. For instance, the stent set with the PDTD configuration leads to higher flow resistance at distal zones of the stent, leading to lower WSS values compared to the case set with the PITD configuration. As consequence, the point in which the radial velocity changes in direction is located at the proximal area of the stent affecting the area where the volumetric blood flow enters and exits the aneurysm sac through the stent.

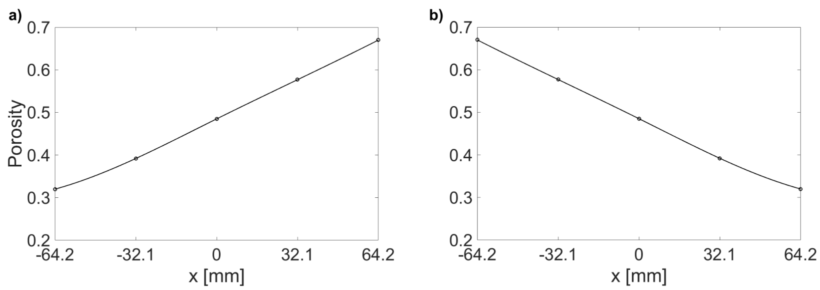

Figure 4.11: Stent porosity configurations: a) Porosity Increasing Toward Distal (PITD) and b) Porosity Decreasing Toward Distal (PDTD)

In summary, the stents with higher stent porosity values increase the velocity of the fluid inside the AAA sac, leading to flow pattern differences at porosity values higher than 0.5. Notably, the point where the radial velocity changes direction shifted distally as the uniform stent porosity increased. This leads to the increase of the local WSS values at distal zones of the AAA wall and differences on the hemodynamic parameters inside the AAA sac. This increment of porosity also affects the other hemodynamic parameters of interest in the same fashion.

Table 4.4 shows how the values of the mass flow and average WSS increase inside the sac as the stent porosity increases. As expected, increasing the stent porosity increases the mass flow into the sac and, consequently, the average WSS. However, note that for non-uniform porosity distributions, the squared pressure difference varies significantly even though the mass flow and wall shear stresses are similar. These results suggest that control of the hemodynamic parameters inside the sac cannot be achieved by intuitively setting the stent porosity, requiring a CFD tool to predict the hemodynamic environment. Currently, there are no clinical practice guidelines to specify which type of porous stent is most efficacious for reducing the AAA progression without increasing the risk of rupture [63]. Therefore the proposed methodology is needed to inform these decisions and to improve clinical outcomes from treatments using porous stents for EVAR of complex

AAAs.

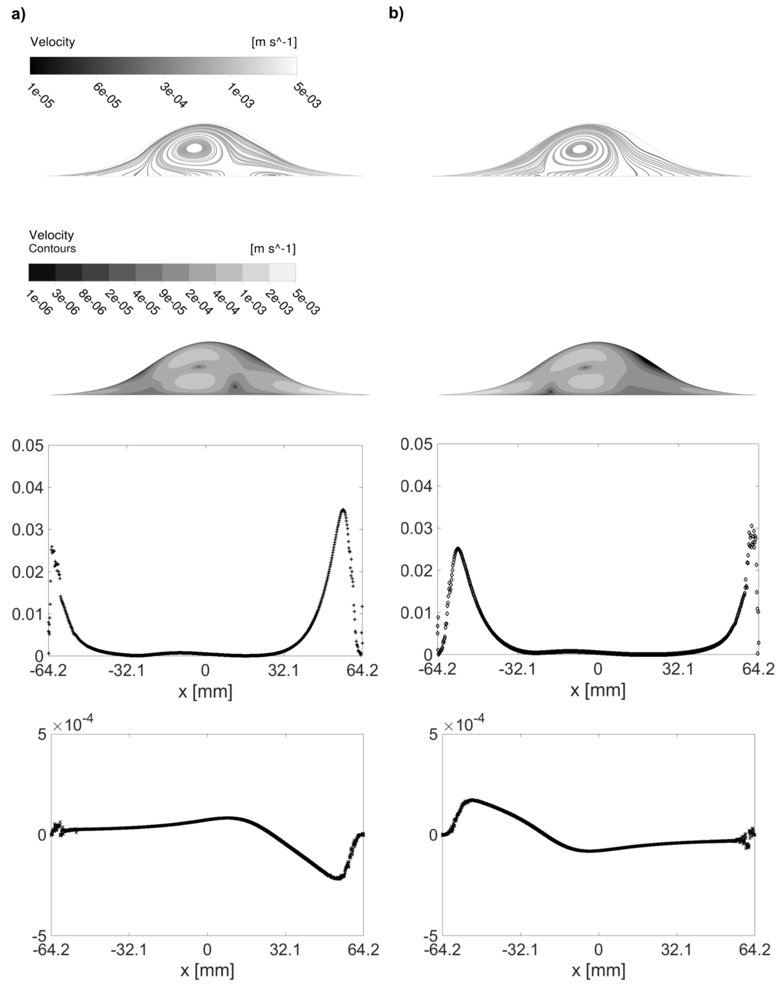

Figure 4.12: Streamlines, isovelocity contours, WSS, and radial velocity across the stent plots corresponding to solutions obtained using the stent configurations in Fig. 4.11

4.4.2 Optimization

From the previous section we observed that designing a stent porosity distribution for inducing specific hemodynamic targets is not a trivial task. It was noted that choice of stent porosity distribution changes the hemodynamics and force distributions inside the AAA sac in complex ways, even more so if we consider patient-specific AAA geometries. Current mathematical, numerical and experimental methods are unable to efficiently

Table 4.4: Mass Flow, Average Wall Shear Stress, and Squared Pressure Difference values attained with the seven cases employed in this study.

Case	$\dot{m}_{sac}$ (l/min)	τ_{avg} (Pa)	$\sum([\Delta P]^2)$ (Pa^2)
UPD_1	0.0049	0.0021	1169.5
UPD_2	0.0103	0.0034	1174.6
UPD_3	0.0382	0.0068	1047.5
UPD_4	0.0801	0.0103	835.5
UPD_5	0.1121	0.0123	749.3
PITD	0.0289	0.0047	2617.5
PDTD	0.0228	0.0041	422.8

determine the best porosity distribution to satisfy hemodynamic targets inside the AAA sac. This situation hinders wider adoption of porous stents.

In an effort to provide further control on the fluid flow inside the AAA sac and improve clinical outcomes, we developed an intelligent approach for finding appropriate stent candidates for any given AAA geometry, as explained in section 4.3. Thus, we selected five of the stent configurations used in the sensitivity study discussed above, UPD_2, UPD_3, UPD_4, PITD, and PDTD, as starting points for the optimization, to demonstrate the efficacy of the proposed design methodology. These initial stent porosity distributions are shown as black lines in the top panels of Figures 4.13 and 4.15, while blue lines show the hemodynamic parameters of interest inside the sac obtained with the final porosity distribution.

The proposed methodology was able to find stent porosity alternatives that minimize the objective function and satisfy the constraints set for the WSS in all cases, demonstrating the ability of controlling the blood flow to achieve specific hemodynamic targets. According to our results, the most commonly observed shape for the final porosity distribution exhibited high porosity values at the center of the stent. However, the methodology was also able to provide other alternatives that also achieved the hemodynamic targets, thus providing flexibility to the designer and/or end users in achieving their objectives.

From the results shown in Figs. 4.13, 4.14, 4.15, and 4.16, we note the existence of

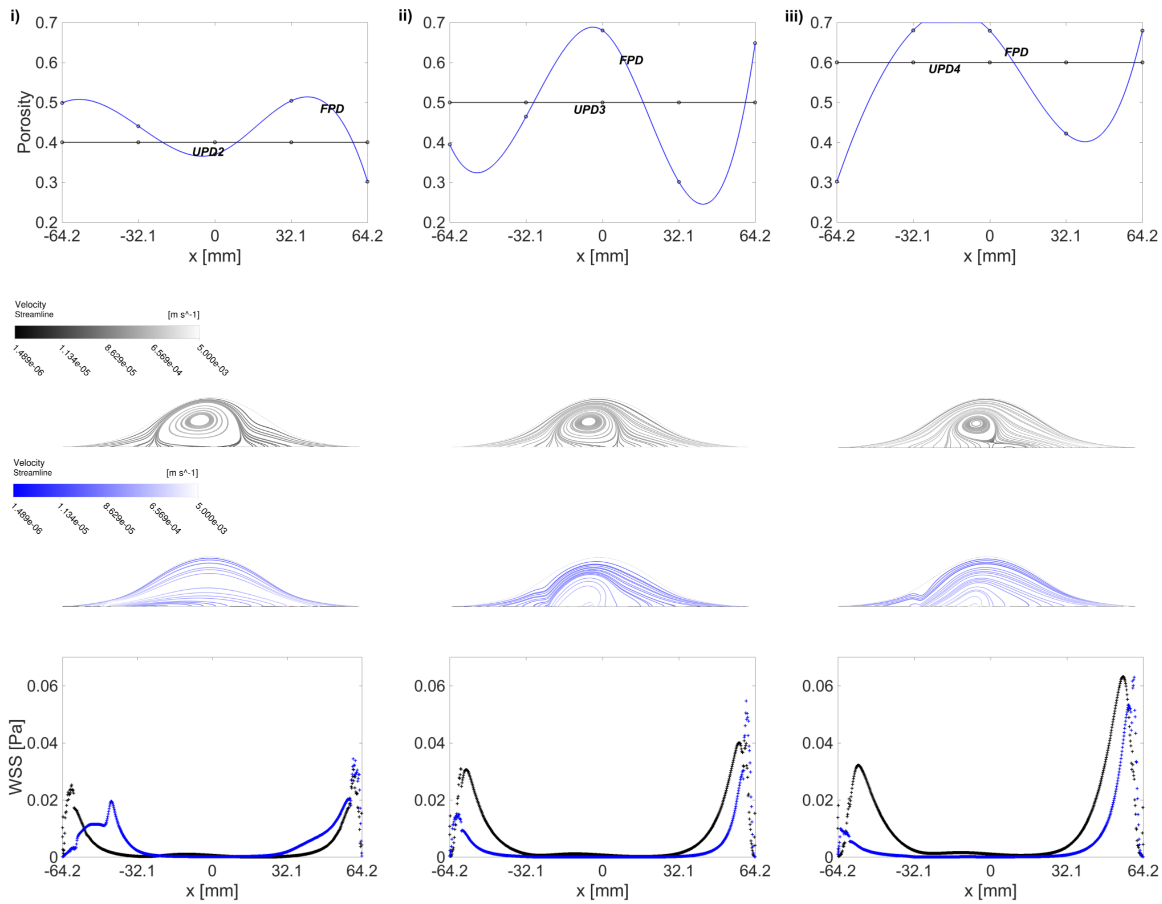

Figure 4.13: Initial (black lines) and final (blue lines) stent porosity distributions (first row), streamlines (second and third row) and WSS (bottom row) resulting from optimization runs with three different initial porosity distributions: i) UPD_2=0.4, ii) UPD_3=0.5,and iii) UPD_4=0.6.

different hemodynamic environments that satisfy the constraints defined for the problem. Different flow patterns are observed for each of the final porosity distributions obtained. Notably, cases ii) and iii) in Fig. 4.13 and case b) in Fig. 4.15 have similar hemodynamic patterns with maximum velocity close to the center of the stent (x=0 mm). Pattern differences are more noted in cases i) and a) of Figs. 4.13 and 4.15 respectively.

Regarding the shape of the final porosity distribution obtained, we can observe similar trend for cases ii) and iii) in Fig. 4.13 and case b) in Fig. 4.15. These cases report higher values of porosity at the center of the stent compared to case i) and a) which show different porosity trends. The high values of porosity at the center of the stent cause

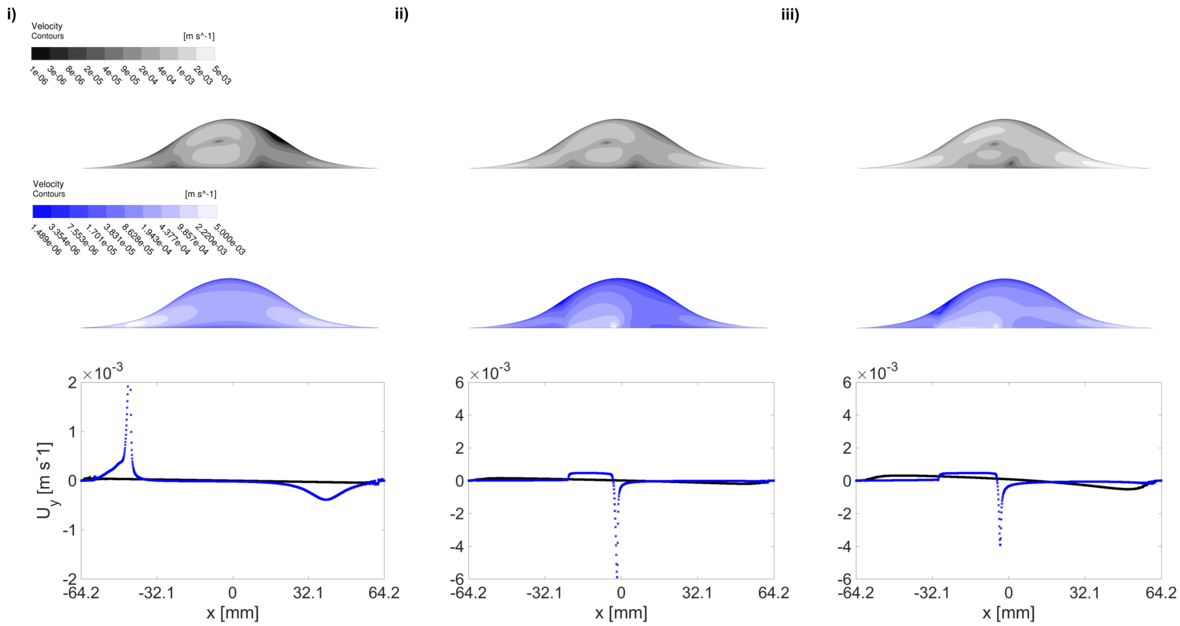

Figure 4.14: Initial (black lines) and final (blue lines) isovelocity contours (first and second rows) and radial velocity across the stent (bottom row) resulting from optimization runs with three different initial porosity distributions: i) UPD_2=0.4, ii) UPD_3=0.5,and iii) UPD_4=0.6.

higher velocities of the fluid around this area. In case a) shown in Fig. 4.15, where the initial distribution of stent was set with the PITD configuration, a minimum and maximum values of porosity were found at the proximal and distal end of the stent, respectively, changing the velocity contour and velocity gradients inside the AAA sac compared to the other results. In addition, from the final porosity distribution results obtained, we note that the stent mode of action is the redirection of the fluid flow in such a way that the flow patterns inside the sac follow the shape of the AAA wall, turning the fluid around a point close to the center of the stent. This point, where the radial velocity is zero, changes position as we change the porosity distribution, for instance, compare the initial (black) and final (blue) streamlines in Figs. 4.13 and 4.15.

Table 4.5 compares the hemodynamic factors of interest obtained with the initial and final porosity distributions. It is noted that all the objective functions were minimized while satisfying the constraint for the shear stress on the aneurysm wall (τ_{avg} < 0.005 Pa). It is important to mention that there were cases in which the constraint for the WSS was

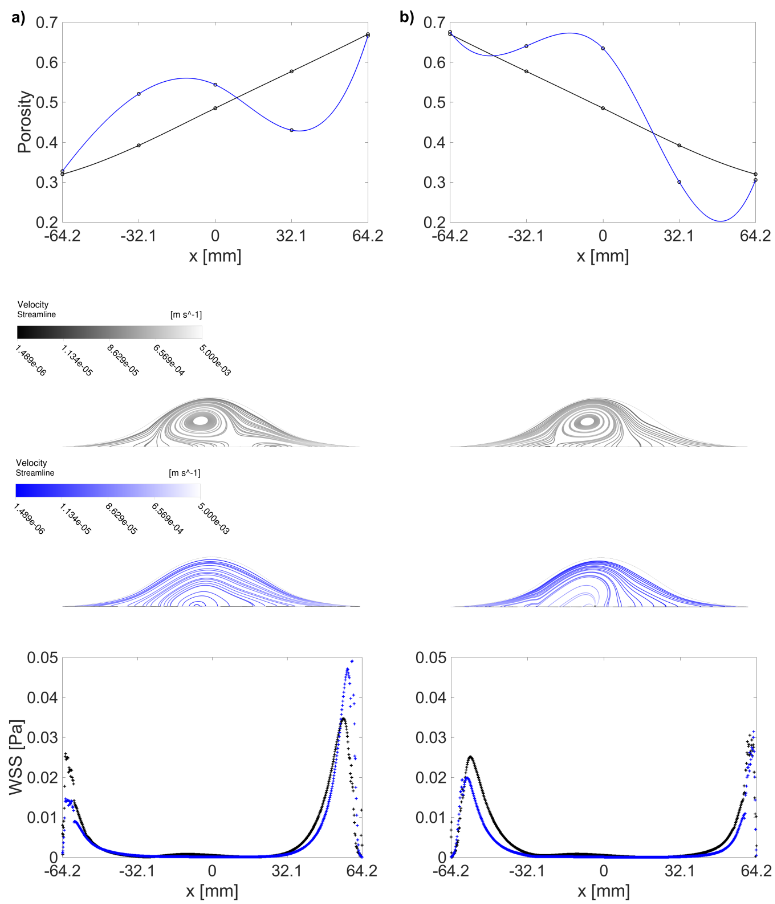

Figure 4.15: Initial (black lines) and final (blue lines) stent porosity distributions (first row), streamlines (second and third row) and WSS (bottom row) resulting from optimization runs with two different initial porosity distributions: a) PITD, and b) PDTD.

satisfied with the initial stent configuration (UPD_2, PDTD, and PITD). Nevertheless, the method was able to keep these values within the range specified while minimizing the objective function.

An important feature of the results shown above is the fact that different initial porosity distributions, once fed into the proposed methodology, may lead to different porosity distributions and the end of the iterations. Although this is an advantage, as it means there are multiple alternatives for the designers or users of the porous stents that meet the hemodynamic targets, there may be situations in which it would be desirable to obtain only one final porosity distribution regardless of the starting point. A possible approach to achieve this would be to constraint specific points inside the AAA sac or

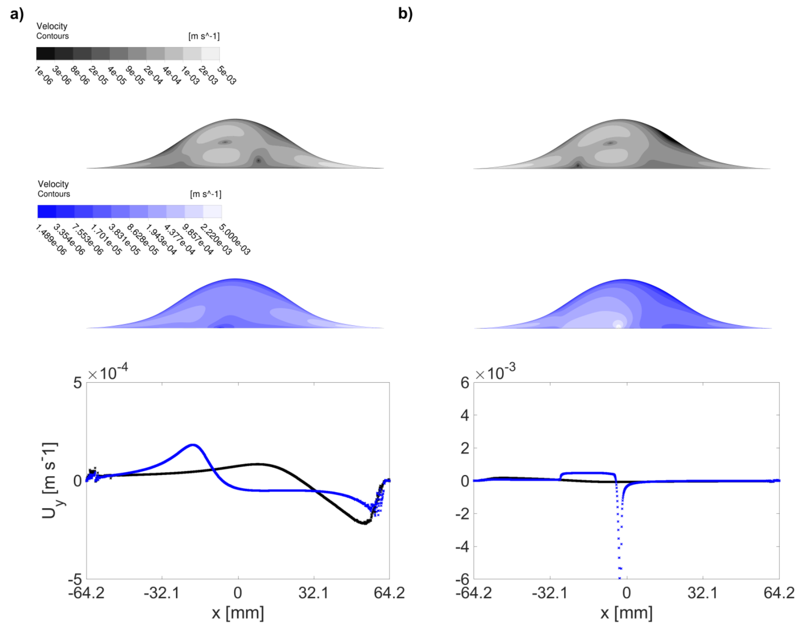

Figure 4.16: Initial (black lines) and final (blue lines) isovelocity contours (first and second rows) and radial velocity across the stent (bottom row) resulting from optimization runs with two different initial porosity distributions: a) PITD, and b) PDTD.

Table 4.5: Hemodynamic results obtained with the initial versus final porosity distribution.

Cases	$\dot{m}_{sac}$ (l/min)		τ_{avg} (Pa)		$\sum([\Delta P]^2)$ (Pa)^2	
	Initial	Final	Initial	Final	Initial	Final
UPD_2	0.010	0.055	0.0034	0.0049	1174	510
UPD_3	0.038	0.051	0.0068	0.0030	1047	465
UPD_4	0.080	0.060	0.0102	0.0045	835	420
PDTD	0.022	0.066	0.0040	0.0028	422	388
PIDT	0.028	0.026	0.0046	0.0045	2617	724

in the AAA wall to reach specific values of WSS, as opposed to the spatially averaged WSS constraint used in the present version of the methodology, Eq. 4.3a. In this thesis, we have refrained from exploring these alternative formulations, limiting ourselves to demonstrate the efficacy of the methodology with the average WSS constraints, without loss of generality.

It is also important to mention that the type of constraint and the parameter ranges defined for this study gives flexibility to the optimization method by allowing more than one hemodynamic pattern as solution. The number of local solutions is restricted according to the range defined for the hemodynamic parameters. Reducing the search range makes finding a unique solution easier (smaller space to search) but could increase the calculation time, making the method impractical from a clinical perspective.

4.4.3 Sensitivity to the Optimization Targets and Constraints

To understand the impact of the initial stent configuration used for starting the optimization on the calculation time, Table 4.6 shows the number of simulations used to obtain the final porosity distribution for each of the initial porosity distributions used.

Table 4.6: Number of function evaluations (i.e., CFD simulations) required to converge during the optimization run.

Cases	Function Evaluations
UPD_1	49
UPD_2	110
UPD_3	98
UPD_4	249
UPD_5	247
PDTD	48
PIDT	38

From Table 4.6, we can observe that the simulation starting from the UPD_4 employed more iterations to reach the final solution, compared to the other cases presented. Additionally, note that the optimization case starting with the PDTD configuration, which yielded the lowest local minimum value of the objective function, did so using the second-lowest number of simulations. Figure 4.17 shows the optimization paths for three optimization cases. Note that in most cases, intermediate results after 10-20 function evaluations are already close to the final solution. The optimization path, however, deviates from the ideal convergence curves, an issue possibly caused by errors introduced by finite-difference approximations of the gradient and Hessian of the objective function.

From a methodological point of view, prior simulations using different porous distribution should be performed before running the optimization to help determine which case is closest to the targets, so as to improve the efficiency of the methodology by decreasing the number of function evaluations and computational time.

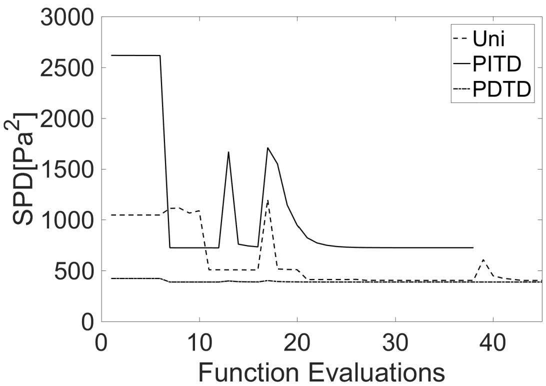

Figure 4.17: Optimization path using as starting point the UDP_3, PIDT, and PDTD stent configurations.

Complementarily, another study to determine the sensitivity of the results to changes on the WSS target range was performed. The PDTD initial stent configuration was used and the WSS constraint was varied by $\pm 10\%$. The final porosity distributions obtained did not show significant variation, indicating that small changes on the constraint do not change the final porosity distribution because the solution does not lie on the constraint boundaries, as can be observed by inspecting the fourth column of Table 4.5.

The proposed methodology successfully found optimized stent porosity distributions using the five knot points uniformly distributed along the stent. The study cases showed that the parametrization used was appropriate to cover a wide range of stent porosity designs. The objective function was minimized, satisfying the WSS constraint required in all cases. However, it was not possible to obtain a unique stent porosity trend, although three of the five study cases showed similar trends leading to similar hemodynamic behavior inside the sac. The solution on these cases showed a wave-shaped porosity distribution with lower porosity at the proximal end of the stent, which decreased the flow velocity and WSS as consequence of the higher flow resistance at that zone, followed by an increase of the stent porosity achieving a maximum value at the center, which increased the flow velocity compared to other zones of the AAA sac. Comparing these three cases with the other solutions, we noted that the amplitude of the wave-shaped porosity distribution plays an important role in the control of the fluid flow. Cases with lower porosity variations along the stent led to different hemodynamic environments inside the AAA sac, even when the objective function was minimized and the constraints satisfied. A stricter formulation for controlling flow parameters at specific points in time or space could narrow the spectra of final solutions, though at the price of larger computational cost.

Chapter 5

General Conclusions

Computational mechanics and fluid dynamic studies were carried out with the aim of developing a methodology to design porous stents for EVAR of complex AAAs. The mechanical study was performed to understand the impact of incomplete intraluminal thrombus (ILT) attachment on the peak stress of the AAA wall. This study was carried out running computational static and fluid-structure interaction simulations assuming hyperelastic isotropic properties for the physiological structures, keeping constant the thickness of the AAA wall. The simulations were run under a constant, fluid-induced pressure distribution along the internal wall of the system. Results from this investigation showed that partially attached ILTs do not increase the AAA wall stress. The fluid flow study was conducted on a 2D hypothetical AAA geometry under steady-state and pulsatile flow conditions using the Navier-Stokes equations for incompressible, laminar flow of a Newtonian fluid with average human blood properties.

Previous works on porous stents used for EVAR have focused on the hemodynamic effect inside the sac for different stent porosity configurations. The results from the majority of those investigations have shown that the blood flow velocities inside the AAA sac are reduced with the presence of stents, as expected. However, it is difficult to control the hemodynamic behaviour inside the sac by choosing arbitrary stent designs. This problem is even more difficult if we consider that the AAA geometry of patient-specific subjects are complex and all geometrically different, making it impossible to determine, *a priori*, a suitable stent design that will provide the hemodynamic behavior required to slow the progression of the pathology. Therefore, to overcome this limitation, we developed a methodology that is able to find stent configurations that ensure better hemodynamic control inside the AAA sac for reducing rupture risks and improving treatment outcomes. In the following paragraphs, we summarize our main research findings.

An investigation to understand the role of the ILT on the distribution and peak stress of the AAA wall was performed. Although previous work reported in the literature has focused on elucidating the mechanical role of ILTs in AAAs, there have been no attempts to model the effect of incomplete ILT attachment to the AAA wall. Our study was performed using the material models developed by Raghavan and Van de Geest [50, 73] for the AAA wall and ILT, respectively, and consisted on CSS and FSI simulations under a constant and fluid-induced pressure distribution along the AAA wall. It was observed that the peak stress on the AAA wall decreases as the attachment area of the ILT decreases. A maximum peak stress difference of 3.5 % was observed when comparing the fully detached and fully attached ILT cases, concluding that partial ILT attachments are not harmful to the protection of the AAA wall. In addition, no significant difference on the peak stress was noted between the CSS and FSI simulation cases which could simplify future studies by just running CSS simulations. The results suggest that incomplete ILT attachment cases are more beneficial for the AAA wall protection than complete ILT attachment cases. Based on these findings, concerns about the ILT attachment type should not be taken into account when designing porous stents for EVAR of complex AAAs. However, this research assumed that the mechanical properties of AAA walls were not affected by the presence of the ILT. As discussed in Chapter 2, thick ILT formations may cause hypoxia which degrades the mechanical properties of the AAA wall, and thus may increase the chances of aneurysm rupture. Full consideration of this effect, however, is hindered by the unavailability of material models that accurately capture this phenomenon.

After performing mechanical studies on AAA and ILT systems to ensure that incomplete ILT attachment types do not cause the reduction of the AAA wall protection, we focussed our research on modelling the presence of the stent as a porous medium. The purpose of this study was to obtain a low cost computational model able to capture the hydrodynamic effect of porous stents, specifically the pressure drop through the stent for different blood flow and stent configurations. The reduction of the computational cost caused by the size difference between the stent pore and the AAA dimension was achieved by performing CFD simulations on detailed pores of the stent varying its configuration to capture the hydrodynamic effect on the coefficients of the porous media model. The results indicated that the pressure drop across the stent increases for high angles of incidence and flow velocities and low wide-screen angles.

Consecutively, we used these results to model the presence of the stent for different configurations to understand the impact of the stent porosity distribution on the hemodynamic parameters inside the AAA sac. The results showed that the hemodynamic parameters depend strongly on the stent porosity distribution, concluding that the hemodynamic control inside the sac is a difficult task to achieve by guessing a suitable stent porosity configuration. We also found stent configurations that negatively changed the hemodynamic conditions inside the sac that may increase the chances of aneurysm wall rupture.

This research has the potential to be applied in studies using patient-specific geometries, reducing computational efforts and improving the accuracy of the results obtained with previous models presented in the literature. In this way, it becomes feasible to conduct pre-clinical assessment of the suitability of a given porous stent for a given patient.

From the CFD study performed to understand the impact of the stent porosity on the hemodynamic parameters inside the stent, we realize that any stent porosity configuration does not ensure an efficient treatment of the pathology. To improve treatment outcomes, CFD simulations employing different stent configurations can be carried out to determine the best alternative. It is important to mention that there were stent porosity cases that led to the inappropriate hemodynamic environment inside the sac. To overcome this problem, a methodology was developed to find stent porosity distributions that control the hemodynamic inside the AAA sac. This methodology which consisted of CFD simulations and an optimization algorithm for modifying the stent porosity every time the hemodynamic targets were not satisfied, was successfully developed. The method was tested under steady-state conditions, finding similar stent porosity trends. The most repetitive stent porosity pattern showed high porosity values at places transversally aligned with the maximum diameter of the AAA. However, alternative stent porosity distributions were found. This research has the potential to be applied to study patient-specific AAA geometries under different flow conditions without loss of generality and can be used for helping future intervention planning to efficiently stop the progression of the pathology.

Porous stents can work by inducing ILTs that would protect AAA walls. These devices were designed to regularize flow pattern, eliminating recirculation zones and shear stresses. We developed a methodology for designing porous stents that control flow parameters inside the AAA sac. We used it to specifically control the blood flow to satisfy hemodynamic factors of the wall within a suitable shear stress range minimizing the increase of pressure that act on the AAA wall. This methodology can be adjusted to control other flow parameters. If more information about the relationship between hemodynamics and thrombus formation were available, we could modify the formulation of the methodology to promote better blood flow and thrombus formation. Some of the steps needed to achieve these aims will be discussed in the next chapter.

Chapter 6

Future Directions

During the development of this research project, we identified some possible research that could improve the understanding of the mode of action of porous stents for EVAR of complex AAAs. In particular, our study was focused on developing a methodology to improve porous stent designs and future guidelines for planning interventions. This methodology was tested on 2D hypothetical AAA geometries under steady-state flow conditions, resulting in a set of different stent porosity distributions that control the blood flow within an specified range of hemodynamic parameters. To further the research objectives, in the following paragraphs we discuss additional studies that would complement the proposed methodology for finding stent porosity distributions.

The methodology that we developed was tested under steady-state conditions and can be employed to study problems with any flow characteristics. Since the blood flow through AAAs is pulsatile by nature, a study employing this flow condition is consequently a next step to explore in the investigation. To perform this study, a physiological, patient-specific pulsatile inlet condition could be employed as a simulation input. The aim of this is to understand the effect of the pulsatile blood flow inside the AAA sac, and how it changes the final porosity distribution obtained with the design methodology with respect to those obtained under steady-state conditions. The problem can be carried out in a similar way as presented in this thesis. That is, the calculation of baseline hemodynamic parameters from simulations on AAAs without the presence of the stent. Then, simulations could be run using different stent configurations to understand their impact on the hemodynamic parameters of interest, and then our proposed design methodology could be applied to obtain suitable stent porosity distributions. Additionally, the transient results can be compared with results obtained from steady-state simulations with the same flow rate, to isolate the impact of the transients on the flow field. This would allow us to verify if the optimal stent designs are similar under steady-state and transient regimes and, if this were the case, to avoid performing transient simulation to design porous stents. This would significantly reduce the computational cost, resulting in shorter timelines that would be consistent with clinical applications.

Another study that can be addressed with the methodology is understanding the effect of the AAA asymmetry on the final stent porosity distribution found by the proposed methodology. To perform this study, we can parameterize a hypothetical AAA geometry so that, by modifying a geometrical factor, we can control the degree of asymmetry of the AAA. For instance, in Fig. 6.1, by varying the factor ϵ, we can generate aneurysm geometries ranging from symmetric ($\epsilon = 1$) to highly asymmetric ($\epsilon = 0.3$).

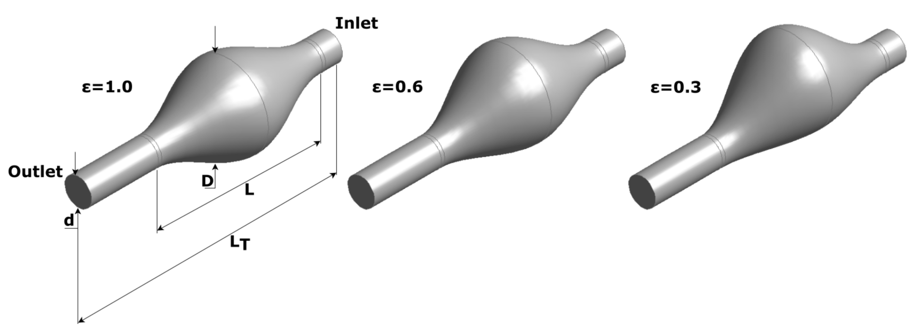

Figure 6.1: Three AAAs of different shapes modified by the geometrical factor ϵ.

To perform this sensitivity study, the geometric models are first simulated without the presence of the stent. These results are compared with simulations using different stent porosity distribution to understand the hemodynamic changes inside the AAA sac as consequence of the presence of the stent. Finally, the methodology is employed to obtain the stent porosity distribution that satisfies the hemodynamic targets.

Since our methodology is not limited by the AAA geometry, a next step in this research would be to perform simulations using patient-specific cases. With this study, we could understand the impact of realistic AAA geometries on the final porosity distribution obtained with the optimization methodology. In case of having AAA systems with more than one outlet, the outlet boundary conditions could be set using a splitting method [61] to improve the hemodynamic predictions by correcting the flow rate at outlet boundaries.

One of the implications of using porous stents for repairing AAAs is the circulation of blood flow inside the AAA sac. The flow control inside the sac can be achieved using the methodology developed in this thesis. However, blood is a fluid plasma with carried particles. In particular, activated platelets are blood components that interact with endothelial cells along the AAA wall, causing ILT formation. Since the formation of this structure is important to control for avoiding unbalanced ILT growth that may negatively impact the mechanical properties of the AAA wall, a study including cell particles could improve predictions and future stent designs. The purpose of such study would be the understanding of the cell particles on the onset of the ILT formation inside the AAA sac. The methodology of study is the tracking of platelets to quantify their stress history during various cardiac cycles that in addition with other hemodynamic parameters can help on the prediction of the ILT formation. This study can help to understand the effect of the porosity distribution obtained with the methodology when particles are included. An interesting metric, the Thrombus Formation Potential (TFP), developed by Achille *et al.* [13], can be employed to predict the thrombus formation. The TFP combines the Platelet Activation Potential, the Oscillatory Shear Index, and the Time Averaged Wall Shear Stress. The purpose is to find the stent porosity distribution that improve thrombogenesis while minimizing the risk of AAA wall rupture caused by flow dynamics inside the AAA sac. If needed, the formulation of optimization should include the TFP into the constraints to control the ILT onset inside the AAA sac homogeneously along the wall. In addition, vorticity and shear strain rate gradients are hemodynamic parameters that could be controlled. By incorporating them into the design methodology with the aim of reducing their intensities, the flow is laminarized under a smoother shear strain rate environment. This consequently promotes more uniform ILT formations along the AAA wall sac, decreasing the chances of thick ILT local formation, improving proteolytic activity, and stopping the progression of the pathology in less time [63, 69].

Bibliography

[1] R. Adolph, D. A. Vorp, D. L. Steed, M. W. Webster, M. V. Kameneva, and S. C. Watkins. Cellular content and permeability of intraluminal thrombus in abdominal aortic aneurysm. *Journal of Vascular Surgery*, 25(5):916–926, 1997.

[2] A. Balderi, A. Antonietti, F. Pedrazzini, D. Sortino, C. Vinay, and M. Grosso. Treatment of visceral aneurysm using multilayer stent: two-year follow-up results in five consecutive patients. *Cardiovascular and Interventional Radiology*, 36(5):1256–1261, 2013.

[3] A. Benjelloun, M. Henry, A. Ghannam, C. Vaislic, A. Azzouzi, W. Maazouzi, A. Khlifi, and J. Benamor. Endovascular treatment of a tuberculous thoracoabdominal aneurysm with the multilayer stent. *Journal of Endovascular Therapy*, 19(1):115–120, 2012.

[4] J. Biasetti, T. C. Gasser, M. Auer, U. Hedin, and F. Labruto. Hemodynamics of the normal aorta compared to fusiform and saccular abdominal aortic aneurysms with emphasis on a potential thrombus formation mechanism. *Annals of Biomedical Engineering*, 38(2):380–390, 2010.

[5] J. Biasetti, F. Hussain, P. G. Spazzini, and T. C. Gasser. An integrated fluidochemical model towards modeling the formation of intra-luminal thrombus in abdominal aortic aneurysms. 3:266, 2011.

[6] A. J. Boyd, D. C. Kuhn, R. J. Lozowy, and G. P. Kulbisky. Low wall shear stress predominates at sites of abdominal aortic aneurysm rupture. *Journal of vascular*

surgery, 63(6):1613–1619, 2016.

[7] B. Burke, A. Giannoudis, K. P. Corke, D. Gill, M. Wells, L. Ziegler-Heitbrock, and C. E. Lewis. Hypoxia-induced gene expression in human macrophages: implications for ischemic tissues and hypoxia-regulated gene therapy. *The American Journal of Pathology*, 163(4):1233–1243, 2003.

[8] M. Cavazzuti, M. Atherton, M. W. Collins, and G. S. Barozzi. Non-Newtonian and flow pulsatility effects in simulation models of a stented intracranial aneurysm. *Proceedings of the Institution of Mechanical Engineers, Part H: Journal of Engineering in Medicine*, 225(6):597–609, June 2011.

[9] S. Chandra, S. Raut, A. Jana, R. Biederman, M. Doyle, S. Muluk, and E. Finol. Fluid-structure interaction modeling of abdominal aortic aneurysms: the impact of patient-specific inflow conditions and fluid/solid coupling. *Journal of Biomechanical Engineering*, 135(8):81001, August 2013.

[10] C. Darling, C. Messina, D. Brewster, and L. Ottinger. Autopsy study of unoperated abdominal aortic aneurysms. the case for early resection. *Circulation*, 56(3 Suppl):II161–4, 1977.

[11] T. Darsaut, F. Bing, A. Makoyeva, G. Gevry, I. Salazkin, and J. Raymond. Flow diversion to treat aneurysms: the free segment of stent. *Journal of neurointerventional surgery*, pages neurintsurg–2012, 2012.

[12] N. DePaola, M. A. Gimbrone, P. F. Davies, and C. F. Dewey. Vascular endothelium responds to fluid shear stress gradients. *Arteriosclerosis, Thrombosis, and Vascular Biology*, 12(11):1254–1257, 1992.

[13] P. Di Achille, G. Tellides, C. a. Figueroa, and J. D. Humphrey. A haemodynamic predictor of intraluminal thrombus formation in abdominal aortic aneurysms. *Proceedings of the Royal Society A: Mathematical, Physical and Engineering Sciences*, 470(2172):20140163–20140163, oct 2014.

[14] E Di Martino, S Mantero, F Inzoli, G Melissano, D Astore, R Chiesa, and R Fumero.

Biomechanics of abdominal aortic aneurysm in the presence of endoluminal thrombus: experimental characterisation and structural static computational analysis. *European Journal of Vascular and Endovascular Surgery*, 15(4):290–299, 1998.

[15] E. S. Di Martino and D. A. Vorp. Effect of variation in intraluminal thrombus constitutive properties on abdominal aortic aneurysm wall stress. *Annals of Biomedical Engineering*, 31(7):804–809, 2003.

[16] M. M. Dua and R. L. Dalman. Hemodynamic influences on abdominal aortic aneurysm disease: Application of biomechanics to aneurysm pathophysiology. *Vascular Pharmacology*, 53(1):11–21, 2010.

[17] D. F. Elger, D. M. Blackketter, R. S. Budwig, and K. H. Johansen. The influence of shape on the stresses in model abdominal aortic aneurysms. *Transactions-American Society of Mechanical Engineers Journal of Biomechanical Engineering*, 118:326–332, 1996.

[18] E. Ferrero, M. Ferri, A. Viazzo, and F. Nessi. Endovascular treatment of hepatic artery aneurysm by multilayer stents: two cases and one-year follow-up. *Interactive Cardiovascular and Thoracic Surgery*, 13(5):545–7, November 2011.

[19] M. F. Fillinger, S. P. Marra, M. L. Raghavan, and F. E. Kennedy. Prediction of rupture risk in abdominal aortic aneurysm during observation: wall stress versus diameter. *Journal of Vascular Surgery*, 37(4):724–732, 2003.

[20] M. F. Fillinger, M. L. Raghavan, S. P. Marra, J. L. Cronenwett, and F. E. Kennedy. In vivo analysis of mechanical wall stress and abdominal aortic aneurysm rupture risk. *Journal of Vascular Surgery*, 36(3):589–597, 2002.

[21] E. A. Finol, K. Keyhani, and C. H. Amon. The effect of asymmetry in abdominal aortic aneurysms under physiologically realistic pulsatile flow conditions. *Journal of Biomechanical Engineering*, 125(2):207, 2003.

[22] V. Fontaine, M. P. Jacob, X. Houard, P. Rossignol, D. Plissonnier, E. Angles-Cano, and J. B. Michel. Involvement of the mural thrombus as a site of protease release and

activation in human aortic aneurysms. *American Journal of Pathology*, 161(5):1701–1710, 2002.

[23] T. C. Gasser, G. Görgülü, M. Folkesson, and J. Swedenborg. Failure properties of intraluminal thrombus in abdominal aortic aneurysm under static and pulsating mechanical loads. *Journal of Vascular Surgery*, 48(1):179–188, July 2008.

[24] L. P. Harter, B. H. Gross, P. W. Callen, and R. A. Barth. Ultrasonic evaluation of abdominal aortic thrombus. *Journal of Ultrasound in Medicine*, 1(8):315–318, 1982.

[25] M. Henry, A. Benjelloun, and I. Henry. A new concept of stent: The multilayer flow modulator. first human study in thoraco abdominal and abdominal aortic aneurysms. *Journal of the American College of Cardiology*, 60(17):B35–B36, October 2012.

[26] M. Henry, A. Benjelloun, and I. Henry. The multilayer flow modulator stent (mfm) for the treatment of complex aortic aneurysms. indicationscontraindications results. *Journal of Indian College of Cardiology*, 7(Supplement 1):S48 – S56, 2017. SI: Lectures from 8th Asia Pacific Vascular Intervention Course (APVIC VIII), 17th19th June 2016, New Delhi, India.

[27] M. Henry, A. Polydorou, N. Frid, P. Gruffaz, A. Cavet, I. Henry, M. Hugel, D. A. Rüfenacht, L. Augsburger, M. De Beule, et al. Treatment of renal artery aneurysm with the multilayer stent. *Journal of Endovascular Therapy*, 15(2):231–236, 2008.

[28] M. Kazi, J. Thyberg, P. Religa, J. Roy, P. Eriksson, U. Hedin, and J. Swedenborg. Influence of intraluminal thrombus on structural and cellular composition of abdominal aortic aneurysm wall. *Journal of Vascular Surgery*, 38(6):1283–1292, 2003.

[29] D. N. Ku. Blood flow in arteries. *Annual Review of Fluid Mechanics*, 29(1):399–434, 1997.

[30] A. M. Lazaris, A. N. Maheras, and S. N. Vasdekis. A multilayer stent in the aorta may not seal the aneurysm, thereby leading to rupture. *Journal of Vascular Surgery*, 56(3):829–831, September 2012.

[31] H. M. Lazarus. Intraluminal graft device, system and method, November 29 1988. US Patent 4,787,899.

[32] S. Lee and D. Steinman. On the relative importance of rheology for image-based CFD models of the carotid bifurcation. *Journal of Biomechanical Engineering*, 129(2):273–278, April 2007.

[33] M. Levitt, L. Johnson, K. Venkat, C. Geindreau, S. Roscoat, R. Morton, and A. Kim, L. Aliseda. Physiologically-relevant measurements of flow through stents: toward improved models of endovascular cerebral aneurysm treatments. *Summer Biomechanics, Bioengineering and Biotransport Conference*, Seattle, WA, US, June 24 2017.

[34] T. Liou and Y. Li. Effects of stent porosity on hemodynamics in a sidewall aneurysm model. *Journal of Biomechanics*, 41(6):1174–1183, January 2008.

[35] I. Lobanov and T. K. Starozhilova. The effect of convective flows on blood coagulation processes. *Pathophysiology of Haemostasis and Thrombosis*, 34(2-3):121–134, January 2005.

[36] C. Lowe, A. Worthington, F. Serracino-Inglott, R. Ashleigh, and C. McCollum. Multi-layer flow-modulating stents for thoraco-abdominal and peri-renal aneurysms: the uk pilot study. *European Journal of Vascular and Endovascular Surgery*, 51(2):225–231, 2016.

[37] E. V. Lugovskoi, P. G. Gritsenko, and S. V. Komisarenko. Molecular mechanisms of the polymerization of fibrin and the formation of its three-dimensional network. *Russian Journal of Bioorganic Chemistry*, 35(4):393–410, July 2009.

[38] M. Makaroun. Mechanical properties and microstructure of intraluminal thrombus from abdominal aortic aneurysm. *Journal of Biomechanical Engineering*, 123(6):536–539, June 2001.

[39] J. T. McPhee, J. S. Hill, and M. H. Eslami. The impact of gender on presentation, therapy, and mortality of abdominal aortic aneurysm in the united states, 2001-2004.

Journal of Vascular Surgery, 45(5):891–899, 2007.

[40] G. Moiseyev, S. Givli, and P. Z. Bar-Yoseph. Fibrin polymerization in blood coagulation-a statistical model. *Journal of Biomechanics*, 46(1):26–30, January 2013.

[41] L Morris, P Delassus, M Walsh, and T McGloughlin. A mathematical model to predict the in vivo pulsatile drag forces acting on bifurcated stent grafts used in endovascular treatment of abdominal aortic aneurysms (aaa). *Journal of biomechanics*, 37(7):1087–1095, 2004.

[42] S. C. Nicholls, J. B. Gardner, M. H. Meissner, and K. H. Johansen. Rupture in small abdominal aortic aneurysms. *Journal of Vascular Surgery*, 28(5):884–888, 1998.

[43] J. C. Parodi, J. Palmaz, H. D. Barone, A. Alvarez, D. Balbachián, and C. Chialduzi. Tratamiento endoluminal de los aneurismas de aorta abdominal. *Actas Cardiovasc*, 1(1):49–55, 1990.

[44] M. I. Patel, D. T. A. Hardman, C. M. Fisher, and M. Appleberg. Current views on the pathogenesis of abdominal aortic aneurysms. *Journal of the American College of Surgeons*, 181(4):371–382, 1995.

[45] T. W. Peach, K. Spranger, and Y. Ventikos. Towards predicting patient-specific flow-diverter treatment outcomes for bifurcation aneurysms: From implantation rehearsal to virtual angiograms. *Annals of Biomedical Engineering*, 44(1):99–111, 2016.

[46] C. C. Pieper, C. Meyer, F. Verrel, H. H. Schild, and K. E. Wilhelm. Using the multilayer stent as a supplement to evar in combined abdominal aortic aneurysm and iliac artery aneurysm with inadequate distal landing zonea case report. *Vascular and Endovascular Surgery*, 46(7):565–569, 2012. PMID: 22914854.

[47] C. Pinto, G. Garas, L. Harling, A. Darzi, R. Casula, and T. Athanasiou. Is endovascular treatment with multilayer flow modulator stent insertion a safe alternative to open surgery for high-risk patients with thoracoabdominal aortic aneurysm? *Annals of Medicine and Surgery*, 15:1–8, 2017.

[48] S. Polzer, T. C. Gasser, J. Swedenborg, and J. Bursa. The impact of intraluminal thrombus failure on the mechanical stress in the wall of abdominal aortic aneurysms. *European Journal of Vascular and Endovascular Surgery*, 41(4):467–473, 2011.

[49] M. Raghavan, J. Kratzberg, and E. S. da Silva. Heterogeneous, variable wall-thickness modeling of a ruptured abdominal aortic aneurysm. In *ASME 2004 International Mechanical Engineering Congress and Exposition*, pages 271–272. American Society of Mechanical Engineers, 2004.

[50] M. L. Raghavan and D. A. Vorp. Toward a biomechanical tool to evaluate rupture potential of abdominal aortic aneurysm : identification of a finite strain constitutive model and evaluation of its applicability. 33(4):475–482, 2000.

[51] M. Raschi, F. Mut, R. Löhner, and J. R. Cebral. Strategy for modeling flow diverters in cerebral aneurysms as a porous medium. *International Journal for Numerical Methods in Biomedical Engineering*, (30):909–925, 2014.

[52] J. Raymond, T. E. Darsaut, A. Makoyeva, F. Bing, and I. Salazkin. Endovascular treatment with flow diverters may fail to occlude experimental bifurcation aneurysms. *Neuroradiology*, 55(11):1355–1363, 2013.

[53] P. Rissland, Y. Alemu, S. Einav, J. Ricotta, and D. Bluestein. Abdominal aortic aneurysm risk of rupture: patient-specific FSI simulations using anisotropic model. *Journal of Biomechanical Engineering*, 131(3):031001, March 2009.

[54] I. N. Roy, A. M. Millen, S. M. Jones, S. R. Vallabhaneni, J. R. H. Scurr, R. G. McWilliams, J. A. Brennan, and R. K. Fisher. Long-term follow-up of fenestrated endovascular repair for juxtarenal aortic aneurysm. *British Journal of Surgery*, 104(8):1020–1027, 2017.

[55] J. Roy, F. Labruto, M. O. Beckman, J. Danielson, G. Johansson, and J. Swedenborg. Bleeding into the intraluminal thrombus in abdominal aortic aneurysms is associated with rupture. *Journal of Vascular Surgery*, 48(5):1108–1113, 2008.

[56] M. A. Ruffino and C. Rabbia. Endovascular repair of peripheral and visceral

aneurysms with the Cardiatis multilayer flow modulator: one-year results from the Italian Multicenter Registry. *Journal of Endovascular Therapy : an official journal of the International Society of Endovascular Specialists*, 19(5):599–610, October 2012.

[57] A. V. Salsac, S. R. Sparks, J. M. Chomaz, and J. C. Lasheras. Evolution of the wall shear stresses during the progressive enlargement of symmetric abdominal aortic aneurysms. *Journal of Fluid Mechanics*, 560:19–51, 2006.

[58] R. M. Sanford, S. A. Crawford, M. G. Doyle, C. Amon, and T. Forbes. Pc226 predicting stent graft rotation in patient-specific abdominal aortic aneurysm repair using computational models. *Journal of Vascular Surgery*, 65(6):200S, 2017.

[59] C. M. Scotti and E. A. Finol. Compliant biomechanics of abdominal aortic aneurysms: a fluid–structure interaction study. *Computers & Structures*, 85(11):1097–1113, 2007.

[60] T. L. T. Shek, L. W. Tse, A. Nabovati, and C. H. Amon. Computational fluid dynamics evaluation of the cross-limb stent graft configuration for endovascular aneurysm repair. *Journal of biomechanical engineering*, 134(12):121002, 2012.

[61] D. Steinman, Ch. Chnafa, O. Brina, and V. M. Pereira. Better than nothing: Arational approach for minimizing the impact of outlet strategy on cerebrovascular simulations. *American Journal of Neuroradiology*, 2017.

[62] J. S. Stockle, D. A. Romero, and C. H. Amon. Promoting Suitable Hemodynamic Conditions for Thrombus Formation in Abdominal Aortic Aneurysms With Multilayer Stents. *ASME International Mechanical Engineering Congress and Exposition*, November 2016.

[63] S. Sultan and N. Hynes. Multilayer flow modulator stent technology: a treatment revolution for us patients?, 2015.

[64] S. Sultan, N. Hynes, E. P. Kavanagh, and E. B. Diethrich. How does the multilayer flow modulator work? the science behind the technical innovation, 2014.

[65] S. Sultan, N. Hynes, and M. Sultan. When not to implant the multilayer flow modulator: Lessons learned from application outside the indications for use in patients with thoracoabdominal pathologies. *Journal of Endovascular Therapy*, 21(1):96–112, 2014.

[66] S. Sultan, E. P. Kavanagh, M. Bonneau, C. Kang, and N. Hynes. Abdominal Aortic Aneurysm Repair Using the Multilayer Flow Modulator in Porcine Animal Models. 3(October 2010):1–10, 2015.

[67] S. Sultan, M. Sultan, and N. Hynes. Early mid-term results of the first 103 cases of multilayer flow modulator stent done under indication for use in the management of thoracoabdominal aortic pathology from the independent global mfm registry. *Journal Cardiovasc Surg (Torino)*, 55(1):21–32, 2014.

[68] J. Swedenborg and P. Eriksson. The intraluminal thrombus as a source of proteolytic activity. *Annals of the New York Academy of Sciences*, 1085(1):133–138, 2006.

[69] J. Swedenborg and P. Eriksson. The intraluminal thrombus as a source of proteolytic activity. *Annals of the New York Academy of Sciences*, 1085:133–138, November 2006.

[70] C. A. Taylor and C. A. Figueroa. Patient-specific modeling of cardiovascular mechanics. *Annual Review of Biomedical Engineering*, 11(1):109–134, 2009.

[71] J. Thubrikar, M. Labrosse, F. Robicsek, J. Al-Soudi, and B. Fowler. Mechanical properties of abdominal aortic aneurysm wall. *Journal of Medical Engineering & Technology*, 25(4):133–142, 2001.

[72] C. D. Vaislic, J. Noël, S. Chocron, J. Robin, V. S. Costache, J. Villemot, J. Marc, P. N. Leprince, T. Unterseeh, E. Portocarrero, et al. One-year outcomes following repair of thoracoabdominal aneurysms with the multilayer flow modulator: report from the strato trial. *Journal of Endovascular Therapy*, 21(1):85–95, 2014.

[73] J. P. Vande Geest, M. S. Sacks, and D. A. Vorp. A planar biaxial constitutive relation for the luminal layer of intra-luminal thrombus in abdominal aortic aneurysms.

Journal of Biomechanics, 39(13):2347–2354, 2006.

[74] J. P. Vande Geest, D. H. J. Wang, S. R. Wisniewski, M. S. Makaroun, and D. A. Vorp. Towards a noninvasive method for determination of patient-specific wall strength distribution in abdominal aortic aneurysms. 34(7):1098–1106, 2006.

[75] A. K. Venkatasubramaniam, M. J. Fagan, T. Mehta, K. J. Mylankal, B. Ray, G. Kuhan, I. C. Chetter, and P. T. McCollum. A comparative study of aortic wall stress using finite element analysis for ruptured and non-ruptured abdominal aortic aneurysms. *European Journal of Vascular and Endovascular Surgery*, 28(2):168–176, 2004.

[76] E. L. G. Verhoeven, G. Vourliotakis, W. T. G. J. Bos, I. F. J. Tielliu, C. J. Zeebregts, T. R. Prins, U. M. Bracale, and J. J. A. M. van den Dungen. Fenestrated stent grafting for short-necked and juxtarenal abdominal aortic aneurysm: an 8-year single-centre experience. *European Journal of Vascular and Endovascular Surgery : the official journal of the European Society for Vascular Surgery*, 39(5):529–36, May 2010.

[77] N. L. Volodos, V. E. Shekhanin, I. P. Karpovich, V. I. Troian, and I. Gur'ev. A self-fixing synthetic blood vessel endoprosthesis. *Vestnik khirurgii imeni II Grekova*, 137(11):123–125, 1986.

[78] D. A. Vorp and J. P. Geest. Biomechanical determinants of abdominal aortic aneurysm rupture. *Arteriosclerosis, thrombosis, and vascular biology*, 25(8):1558–1566, 2005.

[79] D. A. Vorp, P. C. Lee, D. H. J. Wang, M. S. Makaroun, E. M. Nemoto, S. Ogawa, and M. W. Webster. Association of intraluminal thrombus in abdominal aortic aneurysm with local hypoxia and wall weakening. *Journal of Vascular Surgery*, 34(2):291–299, 2001.

[80] D. A. Vorp, W. A. Mandarino, M. W. Webster, and J. Gorcsan III. Potential influence of intraluminal thrombus on abdominal aortic aneurysm as assessed by a

new non-invasive method. *Cardiovascular Surgery*, 4(6):732–739, 1996.

[81] C. Wailliez and G. Coussement. CFD study of multilayer stent hemodynamic effects in abdominal aortic aneurysms. *Journal of Vascular Surgery*, 2013.

[82] D. H. J. Wang, M. Makaroun, M. W. Webster, and D. A. Vorp. Mechanical properties and microstructure of intraluminal thrombus from abdominal aortic aneurysm. *Transaction-American Society of Mechanical Engineers Journal of Biomechanical Engineering*, 123(6):536–539, 2001.

[83] S. Wang, Y. Zhang, J. Feng, Y. Huang, A. Tokgoz, U. Sadat, J. H. Gillard, Q. Lu, and Z. Teng. Influence of overlapping pattern of multiple overlapping uncovered stents on the local mechanical environment: a patient-specific parameter study. *Journal of Biomechanics*, 2017.

[84] P. N. Watton, N. A. Hill, and M. Heil. A mathematical model for the growth of the abdominal aortic aneurysm. *Biomechanics and modeling in mechanobiology*, 3(2):98–113, 2004.

[85] P.N. Watton and N.A. Hill. Evolving mechanical properties of a model of abdominal aortic aneurysm. *Biomechanics and Modeling in Mechanobiology*, 8(1):25–42, 2009.

[86] J. S. Wilson, L. Virag, P. Di Achille, I. Karsaj, and J. D. Humphrey. Biochemomechanics of intraluminal thrombus in abdominal aortic aneurysms. *Journal of Biomechanical Engineering*, 135(2):021011, February 2013.

[87] P. Worth Longest and C. Kleinstreuer. Comparison of blood particle deposition models for non-parallel flow domains. *Journal of Biomechanics*, 36(3):421–430, March 2003.

[88] M. Xenos, S. H. Rambhia, Y. Alemu, S. Einav, N. Labropoulos, A. Tassiopoulos, J. J. Ricotta, and D. Bluestein. Patient-based abdominal aortic aneurysm rupture risk prediction with fluid structure interaction modeling. *Annals of biomedical engineering*, 38(11):3323–3337, 2010.

[89] Z. Xu, N. Chen, M. M. Kamocka, E. D. Rosen, and M. Alber. A multiscale model of

thrombus development. *Journal of the Royal Society, Interface / the Royal Society*, 5(24):705–22, July 2008.

[90] F. Yilmaz, M. Y. Gundogdu, et al. A critical review on blood flow in large arteries; relevance to blood rheology, viscosity models, and physiologic conditions. *Korea-Australia Rheology Journal*, 20(4):197–211, 2008.

[91] L.T. Zhang and M. Gay. Immersed finite element method for fluid-structure interactions. *Journal of Fluids and Structures*, 23(6):839 – 857, 2007.

[92] P. Zhang, A. Sun, F. Zhan, J. Luan, and X. Deng. Hemodynamic study of overlapping bare-metal stents intervention to aortic aneurysm. *Journal of Biomechanics*, 47(14):3524–3530, 2014.